Charge-spin separation and the spectral properties of Luttinger liquids

1993 J. Phys.: Condens. Matter 5 8305

(http://iopscience.iop.org/0953-8984/5/44/020)

J. Phys.: Condens. Matter 5 (1993) 8305–8336. Printed in the UK

Charge–spin separation and the spectral properties of Luttinger liquids

Johannes Voit
Institut Laue–Langevin, BP 156, 38042 Grenoble Cédex 9, France

Received 29 March 1993

Abstract. We compute the spectral function $\rho(q,\omega)$ of the one-dimensional Luttinger model. We discuss the distinct influences of charge–spin separation and of the anomalous dimensions of the fermion operators and their evolution with correlation strength. Charge–spin separation shows up in finite spectral weight at frequencies between $v_\sigma q$ and $v_\rho q$, where v_σ and v_ρ are the velocities of spin and charge fluctuations, while spectral weight above $v_\rho q$ and below $-v_\rho q$ is generated by the hybridization of the Fermi surface at $\pm k_F$ by interactions. There are non-universal power-law singularities at these special frequencies. We discuss the consistency of recent photoemission experiments on low-dimensional conductors with a Luttinger-liquid picture, which then would suggest very strong long-range interactions. It is pointed out that many-particle correlation functions in principle exhibit similar singularities, but they probe different and complementary aspects of the Fermi-surface interactions.

1. Introduction

There are fundamental differences between interacting one-dimensional (1D) fermion systems and three-dimensional (3D) ones. In 3D, Fermi-liquid theory is based on the existence of quasiparticles evolving out of the electrons (holes) of a Fermi gas upon adiabatically switching on interactions. They are in one-to-one correspondence with the bare particles and, specifically, exhibit the same quantum numbers and obey Fermi–Dirac statistics. Fermi-liquid theory describes the vicinity of the 3D Fermi surface, but the quasiparticles are robust against small displacements away from the Fermi surface with a lifetime diverging as $\tau \sim (E-E_F)^{-2}$. Ideally, they dominate the single-particle spectral response with a sharp peak at $\omega = \varepsilon(k)$ becoming broader as $E - E_F$ increases. In addition to the quasiparticles, there are bosonic collective excitations such as charge or spin fluctuations contributing incoherent background to the spectral function. Of course, there may be borderline cases where the quasiparticle peak is weak and most of the spectral weight resides in the incoherent parts.

In 1D, there are no quasiparticles in the vicinity of the Fermi surface and the excitations are gapless bosonic collective modes involving charge and spin degrees of freedom [1]. They usually propagate with different velocities: an incoming electron decays in distinct charge and spin excitations, which spatially separate with time. The quantum numbers are reversed: charge $\pm e$ and spin 0, and spin 1/2 and charge 0, respectively (a situation reminiscent of the solitons in polyacetylene [2]); hence the name charge–spin separation. Correlation functions usually decay as non-universal power laws as a function of x and t and show non-universal singularities as functions of q and ω. All of these features have dramatic consequences for the spectral properties of interacting 1D fermions, which are

0953-8984/93/448305+32$07.50

much less studied than those of the Fermi liquid and which are the subject of the present paper.

All these features—absence of quasiparticles, charge–spin separation, power-law correlations—are generic to 1D fermion systems but are particularly prominent in the exactly solvable Luttinger model [3–6] whose ground state can be viewed as a gas of non-interacting bosons. All its correlation functions can, in principle, be calculated exactly. Based on case studies of Bethe *ansatz* solvable models [7], Haldane conjectured that this picture remains true, at least in terms of renormalized bosons and up to perturbative corrections, for the asymptotic low-energy properties of a much wider class of 1D models, and coined the term 'Luttinger liquid' to describe the universal low-energy phenomenology of gapless 1D quantum systems [8]. There is an obvious analogy to the Fermi-gas and Fermi-liquid pictures in higher dimensions as described above.

Haldane's conjecture has been verified extensively for many 1D lattice models by a variety of methods. The parameters characterizing the Luttinger-liquid fixed point of Bethe *ansatz* solvable models such as the 1D Hubbard model can be identified by comparing quantities that are accessible by both methods [9] or via conformal invariance [10]. A similar procedure has been applied in a numerical study of the 1D t–J model [11] but, surprisingly, these parameters can even be extracted from variational wavefunctions [12]. Perturbative renormalization group theory allows either determination of the Luttinger-liquid parameters or direct calculation of correlation functions [13].

The recent interest in Luttinger liquids is due, to a large extent, to Anderson's proposal that the normal-state properties of the high-T_c superconductors could be described by a hypothetical 'tomographic' Luttinger liquid [14, 15]. Much of this discussion is based on the spectral properties of the high-T_c materials measured by angle-resolved photoemission [16] and the anisotropic transport properties. A central issue there is charge–spin separation. Theoretically, the possibility of Luttinger-liquid behaviour and charge–spin separation in two dimensions is quite controversial [15, 17, 18]. Observe, however, that a variational wavefunction implementing Luttinger-liquid correlations currently produces the best variational energy for the 2D t–J model [19]. On the other hand, the spectral response of even the 1D Luttinger liquid, and, in particular, the manifestation of charge–spin separation there, are only poorly understood.

Experimental evidence for Luttinger-liquid behaviour in quasi-1D systems has been produced in various organic conductors and superconductors. In tetrathiafulvalene-tetracyanoquinodimethane (TTF-TCNQ), for example, there are strong charge-density wave (CDW) fluctuations at wavevector $4k_F$ in addition to those at $2k_F$ [20]—a fact that can be explained only by assuming sizable Coulomb interactions [21]. Moreover, the optical conductivity of TTF-TCNQ is strongly depressed at low frequencies in the normal state [22], in a manner consistent with a single-particle pseudogap, in the case when impurities and phonons are sufficiently efficient in suppressing the ideal Luttinger model's delta-function conductivity. Mainly based on anomalous nuclear magnetic resonance (NMR) relaxation behaviour, a strong case for Luttinger-liquid behaviour has been made for the normal state of the organic superconductors based on tetramethyltetraselenafulvalene ($(TMTSF)_2X$, X=PF_6, AsF_6, ClO_4, ..., 'Bechgaard salts') [23, 24]. The normal-state properties of quasi-1D inorganic CDW materials are much less well understood.

Finally, most recently and synchronously with the present work, photoemission studies have been performed on both some inorganic CDW materials [25–27] and the organic superconductor $(TMTSF)_2PF_6$ [28]. These studies generally show an intriguing absence of spectral weight at the Fermi surface and, in the angle-resolved experiments, no dispersive low-energy feature reminiscent of quasiparticle peaks. It has been suggested [24, 27, 28]

that this could be related to Luttinger-liquid correlations. The similarity of the spectral response is highly surprising given the great dissimilarity in the other physical properties of these two classes of materials. Since the results of the present paper are of direct relevance, I shall comment on this issue in more detail below.

In this paper, I discuss in detail the spectral function of the Luttinger model and its energy-dependent density of states. I shall take care to separate the influences of charge–spin separation and of the power-law correlations characteristic of 1D fermions, in the spectral function. To this end, two important simplifications of the spinful Luttinger model will be discussed: spinless fermions exhibiting power-law correlations but not charge–spin separation; and a one-branch Luttinger model possessing charge–spin separation but no anomalous fermion dimensions. In the next section, these models will be presented together with an outline of the calculation of the single-particle Green function $G(x, t)$. The Fourier transform to the spectral function $\rho(q, \omega)$ and results will be presented in section 3, together with asymptotic formulae for the real parts of the Green functions.

In section 4 we present new results on the energy-dependent density of states of the Luttinger model and of a related model whose charge degrees of freedom are of the Luttinger type but whose spin fluctuations are gapped. These results are a prerequisite for the discussion of section 5, which addresses the possible connection between the present findings and recent photoemission studies on quasi-1D materials. Section 6 will conclude the paper with an investigation of the spectral properties of many-particle correlation functions, which nicely complement the information extracted from single-particle properties. A brief report of this work has appeared earlier [29] as well as independent parallel work by Meden and Schönhammer [30].

2. Model Hamiltonians and Green functions in real space

The Luttinger model [3–5] describes 1D left- and right-moving fermions with linear dispersion through the Hamiltonian

$$H = H_0 + H_2 + H_4 \tag{2.1a}$$

where

$$H_0 = \frac{1}{L}\sum_{r,k,s} v_F(rk - k_F)c^+_{rks}c_{rks} \tag{2.1b}$$

$$H_2 = \frac{1}{L}\sum_{p,s,s'}[g_{2\parallel}(p)\delta_{s,s'} + g_{2\perp}(p)\delta_{s,-s'}]\rho_{+,s}(p)\rho_{-,s'}(-p) \tag{2.1c}$$

$$H_4 = \frac{1}{2L}\sum_{r,p,s,s'}[g_{4\parallel}(p)\delta_{s,s'} + g_{4\perp}(p)\delta_{s,-s'}] : \rho_{r,s}(p)\rho_{r,s'}(-p) : . \tag{2.1d}$$

Here c^+_{rks} creates a fermion with spin s and momentum k on the branch $r = \pm$ of the dispersion $\varepsilon_r(k) = v_F(rk - k_F)$ where v_F is the Fermi velocity, $-\infty < k < \infty$ and all negative energy states are filled.

It is remarkable that this model can be solved exactly even in the presence of the (charge- and spin-current-conserving) interactions H_2 and H_4 with spin-dependent coupling constants $g_{2\parallel,\perp}(p)$ and $g_{4\parallel,\perp}(p)$ coupling the density operators

$$\rho_{r,s}(p) = \sum_k (c^+_{rk+ps}c_{rks} - \delta_{p,0}\langle 0|c^+_{rks}c_{rks}|0\rangle) \tag{2.2}$$

normal ordered (denoted for short by the symbol : ... :) because of the infinite ground-state expectation value of the number operator $\sum_k c^+_{rks}c_{rks}$. As a consequence of the linear dispersion the $\rho_{r,s}$ obey boson commutation relations

$$[\rho_{r,s}(p), \rho_{r',s'}(-p')] = -\delta_{r,r'}\delta_{s,s'}\delta_{p,p'}rpL/(2\pi). \tag{2.3}$$

Introducing operators

$$\nu_r(p) = (1/\sqrt{2})[\rho_{r,\uparrow}(p) \pm \rho_{r,\downarrow}(p)] \tag{2.4}$$

and interaction constants

$$g_{i\nu}(p) = \tfrac{1}{2}[g_{i\parallel}(p) \pm g_{i\perp}(p)] \tag{2.5}$$

for charge ($\nu = \rho$, '+' applies) and spin ($\nu = \sigma$, '−' applies) fluctuations, H separates into a charge and spin part and can be written as a boson bilinear

$$H_0 = \frac{\pi v_F}{L} \sum_{\substack{\nu=\rho,\sigma \\ r,p}} : \nu_r(p)\nu_r(-p) : \tag{2.6a}$$

$$H_2 = \frac{2}{L} \sum_{\substack{\nu=\rho,\sigma \\ p}} g_{2\nu}(p)\nu_+(p)\nu_-(-p) \tag{2.6b}$$

$$H_4 = \frac{1}{L} \sum_{\substack{\nu=\rho,\sigma \\ r,p}} g_{4\nu}(p) : \nu_r(p)\nu_r(-p) : . \tag{2.6c}$$

Equation (2.6) suggests the possibility for an exact solution via a Bogoliubov transformation [5], but an equivalent solution has also been produced by diagrammatic methods [6] using Ward identities.

There have been different cut-off procedures in the literature. An unambiguous one, used throughout what follows, is to impose a cut-off Λ on the momentum transfer of the interactions $g(p)$ [8], producing momentum-dependent $g_i(p)$. The cut-off Λ must be kept finite to ensure a normalizable ground state, although its value is without importance. A comment is in order on the values $g_i(p = 0)$ appearing in later calculations. Generally, for an interaction

$$H_{\text{int}} = \frac{1}{L} \sum_{\substack{k,k',p \\ s,s'}} V_{ss'}(p)c^+_{k+p,s}c^+_{k'-p,s'}c_{k',s'}c_{k,s}$$

the coupling constants $g_i(p)$ are obtained by neglecting the dependence on k and k' and accounting for the antisymmetry of the fermion operators:

$$g_{2ss'}(p) = \lim_{k\to\pm k_F} \lim_{k'\to\mp k_F} \tfrac{1}{2}[V_{ss'}(p) - V_{ss'}(k + p - k')\delta_{s,s'}]$$

$$g_{4ss'}(p) = \lim_{k\to\pm k_F} \lim_{k'\to\pm k_F} \tfrac{1}{2}[V_{ss'}(p) - V_{ss'}(k + p - k')\delta_{s,s'}].$$

In general, $g_i(0)$ will be finite. However, $g_{4\parallel} = 0$ implying that no non-trivial scattering can originate from this interaction. This is simply seen by crossing the legs in a diagrammatic representation. Choosing a finite $g_{4\parallel}$ will only produce a renormalization of the single-particle properties such as v_ρ and v_σ (below). Notice that $g_{4\parallel} = 0$ with $g_{4\perp}$ finite is fully compatible with spin-rotation invariance.

After diagonalization, we have from equations (2.1) or (2.6)

$$H = \frac{\pi}{L} \sum_{\substack{\nu=\rho,\sigma \\ r,p}} v_\nu(p) : \tilde{\nu}_r(p)\tilde{\nu}_r(-p) : \tag{2.7}$$

where the renormalized velocity of the collective excitations is given as

$$v_\nu(p) = \{[v_F + g_{4\nu}(p)/\pi]^2 - [g_{2\nu}(p)/\pi]^2\}^{1/2}. \tag{2.8}$$

For $g_{4\perp} \neq 0$ we find $v_\rho \neq v_\sigma$, making apparent that charge and spin fluctuations propagate with different velocities. Charge–spin separation is a manifest property of the Luttinger model, equations (2.6), while in more realistic theories it is dynamically generated in the vicinity of the Fermi surface and holds for the asymptotic low-energy properties [9, 10, 14, 15, 31]. In addition, there is a stiffness constant

$$K_\nu(p) = \{[\pi v_F + g_{4\nu}(p) - g_{2\nu}(p)]/[\pi v_F + g_{4\nu}(p) + g_{2\nu}(p)]\}^{1/2} \tag{2.9}$$

governing the long-distance decay of correlation functions. $K_\sigma = 1$ for spin-rotation-invariant problems. The non-universal quantities v_ν and K_ν completely describe the physics of the model. The Luttinger-liquid hypothesis postulates that renormalized v_ν and K_ν also describe the asymptotic low-energy physics of more realistic 1D quantum systems provided they have massless excitations [7] and that, to lowest order, relations between different correlation functions, expressed in the (non-universal) K_ν and v_ν, are universal there.

While our main interest is targeted at the spinful Luttinger model, equations (2.1) and (2.6), we shall also discuss two toy problems to separate power-law correlations from charge–spin separation in the spectral functions below. Spinless fermions can have non-trivial exponents $K_0 \neq 1$ but have only one velocity v_0. If $g_{2\rho} = g_{2\sigma} = 0$ the two branches of the Luttinger model decouple. Then $K_\rho = K_\sigma = 1$, i.e. the same value as for free fermions. The remaining $g_{4\perp} \neq 0$ will however yield $v_\rho \neq v_\sigma$, i.e. a minimal model for charge–spin separation. Even such a simplified model has physical relevance, e.g. for the edge state responsible for transport in the quantum Hall effect where the strong magnetic field gives a definite chirality to the particles and the spin degrees of freedom survive under certain circumstances [32]. Moreover, it has been conjectured that a related problem is exactly solvable even on a lattice [33].

We wish to calculate the spectral function

$$\rho_{rs}(q, \omega) = -(1/\pi)\,\mathrm{Im}\, G^R_{rs}(k_F + q, \omega + \mu) \tag{2.10}$$

where $G^R_{rs}(k_F + q, \omega + \mu)$ is the Fourier transform of the retarded Green function

$$G^R_{rs}(x; t) = -i\theta(t)(\{\psi_{rs}(xt), \psi^+_{rs}(00)\}). \tag{2.11}$$

$\psi_{rs}(xt)$ describes fermions in real space, $\{\ldots, \ldots\}$ denotes the anticommutator, and μ is the chemical potential. ψ_{rs} is related to the bosons $\nu_r(p)$ via Haldane's bosonization identity [8]

$$\psi_{rs}(x) = \lim_{\alpha \to 0} \frac{\exp(irk_F x)}{(2\pi\alpha)^{1/2}} U^+_{r,s} \exp\left(\frac{-i}{\sqrt{2}}\{r\phi_\rho(x) - \theta_\rho(x) + s[r\phi_\sigma(x) - \theta_\sigma(x)]\}\right) \tag{2.12a}$$

(a similar expression was derived in [34]) through bosonic phase fields

$$\phi_\nu(x) = -\frac{i\pi}{L} \sum_{p \neq 0} \frac{\exp(-\alpha|p|/2 - ipx)}{p} [\nu_+(p) + \nu_-(p)] - (N_{+,\nu} + N_{-,\nu})\frac{\pi x}{L} \tag{2.12b}$$

$$\theta_\nu(x) = -\frac{i\pi}{L} \sum_{p \neq 0} \frac{\exp(-\alpha|p|/2 - ipx)}{p} [\nu_+(p) - \nu_-(p)] + (N_{+,\nu} - N_{-,\nu})\frac{\pi x}{L}. \tag{2.12c}$$

$U_{r,s}$ is a fermionic ladder operator and $N_{r,\nu}$ are the $q = 0$ components of the density operators.

Equation (2.11) is then evaluated as

$$G^{\mathrm{R}}_{r,s}(x,t) = -\mathrm{i}\frac{\theta(t)}{2\pi}\exp(\mathrm{i}rk_{\mathrm{F}}x)\lim_{\alpha\to 0}\left[\frac{\Lambda+\mathrm{i}(v_{\mathrm{F}}t-rx)}{\alpha+\mathrm{i}(v_{\mathrm{F}}t-rx)}\right.$$
$$\left.\times\prod_{\nu=\rho,\sigma}\frac{1}{[\Lambda+\mathrm{i}(v_\nu t-rx)]^{1/2}}\left(\frac{\Lambda^2}{(\Lambda+\mathrm{i}v_\nu t)^2+x^2}\right)^{\gamma_\nu}+\begin{pmatrix}x\to -x\\ t\to -t\end{pmatrix}\right]. \tag{2.13}$$

Here

$$\gamma_\nu = (K_\nu + K_\nu^{-1} - 2)/8 \tag{2.14}$$

with

$$K_\nu = \lim_{p\to 0} K_\nu(p) \qquad \text{and} \qquad v_\nu = \lim_{p\to 0} v_\nu(p).$$

Equation (2.13) agrees with Suzumura [35], and is exact to logarithmic accuracy, i.e. in the power laws. Corrections of order $\exp(x^{-1}, t^{-1})$ depending on details of the interactions have, however, been neglected. Notice that $G(x,t)$ and thus all single-particle properties depend only on the exponent γ_ν and the velocities v_ν. The exponents γ_ν mainly measure the strength of the interaction but do not distinguish between attraction and repulsion ($K_\nu \to K_\nu^{-1}$ upon $g_2 \to -g_2$). Λ sets the scale for the crossover from free-fermion behaviour for $|x|, |t| \ll \Lambda$ to Luttinger-liquid decay in the opposite limit. The first factor in square brackets is a consequence of accounting for the momentum dependence of $v_\nu(p)$ and $K_\nu(p)$ and of vital importance for the correct behaviour of the spectral function at large frequency and wavevector. In some cases, one may wish to work with approximate expressions neglecting the p dependence of v_ν and K_ν. There equation (2.13) reduces to

$$G^{\mathrm{R}}_{r,s}(x,t) = -\mathrm{i}\frac{\theta(t)}{2\pi}\exp(\mathrm{i}rk_{\mathrm{F}}x)\lim_{\alpha\to 0}\left[\prod_{\nu=\rho,\sigma}\frac{1}{[\alpha+\mathrm{i}(v_\nu t-rx)]^{1/2}}\right.$$
$$\left.\times\left(\frac{\Lambda^2}{(\Lambda+\mathrm{i}v_\nu t)^2+x^2}\right)^{\gamma_\nu}+\begin{pmatrix}x\to -x\\ t\to -t\end{pmatrix}\right]. \tag{2.15}$$

This approximation has been employed frequently [29,30,36]. For spinless fermions, $G^{\mathrm{R}}_{r,s}(x,t)$ can be obtained from (2.13) and (2.15) by replacing the σ contributions by another ρ contribution of the same structure, while the one-branch Luttinger liquid is simply generated by setting $\gamma_\nu \equiv 0$.

3. Results: $G(k,\omega)$

The principal problem remaining is the Fourier transformation of equation (2.13),

$$G^{\mathrm{R}}_{r,s}(k,\omega) = \int_{-\infty}^{\infty}\mathrm{d}x\int_{-\infty}^{\infty}\mathrm{d}t\exp[-\mathrm{i}(kx-\omega t)]G^{\mathrm{R}}_{rs}(x,t).$$

I have failed to perform this transformation exactly for the generic model, equation (2.13). Serious difficulties arise in the computation of the real parts (to be discussed in section 3.2) and when more than two velocities are present. Progress is possible for the calculation of

the spectral function, $\rho_r(q,\omega) = -(1/\pi)\,\mathrm{Im}\,G^{\mathrm{R}}_{rs}(k_{\mathrm{F}}+q,\omega+\mu)$, equation (2.10), using the property

$$[G^{\mathrm{R}}_{rs}(k,\omega)]^* = -G^{\mathrm{R}}_{rs}(-k,-\omega). \tag{3.1}$$

The spectral function obeys the sum rule

$$\int_{-\infty}^{\infty} \mathrm{d}\omega\, \rho_r(q,\omega) = 1 \qquad \text{for all } q \tag{3.2}$$

which has been verified for all the results presented below where not stated explicitly to the contrary. Two important quantities can be derived directly from the spectral and time-ordered Green function. The single-particle density of states

$$N(\omega) = \sum_r \int_{-\infty}^{\infty} \frac{\mathrm{d}q}{2\pi} \rho_r(q,\omega) \tag{3.3}$$

behaves asymptotically ($\omega \to 0$) as

$$N(\omega) \sim |\omega|^{\alpha}. \tag{3.4}$$

The momentum distribution function

$$n(k) = -\mathrm{i}\sum_r \int_{-\infty}^{\infty} \mathrm{d}x\, \mathrm{e}^{-\mathrm{i}kx} G_{r,s}(x,0^-) \tag{3.5}$$

is derived from the time-ordered Green function, and varies as

$$n(k_{\mathrm{F}}+q) \simeq \tfrac{1}{2} - C_1\,\mathrm{sgn}(q)|q|^{\alpha} - C_2 q \qquad \text{for } q \ll k_{\mathrm{F}}. \tag{3.6}$$

The exponent α characterizes all single-particle properties and is given by

$$\alpha = 2(\gamma_\rho + \gamma_\sigma). \tag{3.7}$$

It has played an important role in the recent discussion about the Luttinger-liquid description of 1D lattice models [7–10, 31]. For the repulsive Hubbard model off half-filling, $\alpha < 1/8$ [7], where $\alpha = 1/8$ is reached for infinite U. More detailed calculations of these quantities are reported below. Because of its key role in the past, α will be used throughout for labelling the figures where we limit ourselves to the spin-rotation-invariant case $\gamma_\sigma = 0$.

3.1. Spectral functions

We shall discuss, in order, spinless fermions, the one-branch Luttinger model and the spinful model to gain an understanding of the roles of anomalous dimensions and charge–spin separation, respectively.

3.1.1. Spinless Luttinger model. We begin with spinless fermions. The spinless Luttinger model allows us to study the influence of the anomalous dimensions of fermions without charge–spin separation. This problem has been considered previously in an approximate manner by Luther and Peschel [36] based on equation (2.15). It is interesting to reconsider this simple problem also because the crossover to the high-energy limit $q \gg \Lambda^{-1}$ can be studied in a fairly complete and detailed manner using the Green function (2.13). We introduce new variables

$$s = v_0 t - rx \qquad s' = v_0 t + rx \tag{3.8}$$

and obtain, using (3.1),

$$\rho_r(q,\omega) = \frac{1}{8\pi^2 v_0 \Lambda} \int_{-\infty}^{\infty} \mathrm{d}s \int_{-\infty}^{\infty} \mathrm{d}s' \exp(\mathrm{i}\Omega_1 s) \exp(\mathrm{i}\Omega_2 s') \times \lim_{\alpha \to 0} \left[\frac{\Lambda + \mathrm{i}(a_F s + b_F s')}{\alpha + \mathrm{i}(a_F s + b_F s')} \left(\frac{\Lambda}{\Lambda + \mathrm{i}s} \right)^{\gamma_0 + 1} \left(\frac{\Lambda}{\Lambda + \mathrm{i}s'} \right)^{\gamma_0} + \begin{pmatrix} s \to -s \\ s' \to -s' \end{pmatrix} \right] \tag{3.9}$$

where the following new quantities have been defined:

$$q = k - rk_F \qquad \Omega_1 = \omega/2v_0 + rq/2 \qquad \Omega_2 = \omega/2v_0 - rq/2$$
$$a_F = \tfrac{1}{2}(v_F/v_0 + 1) \qquad b_F = \tfrac{1}{2}(v_F/v_0 - 1).$$

γ_0 and v_0 are defined similar to equations (2.8), (2.9) and (2.14) by

$$\begin{aligned} v_0 &= [v_F^2 - (g_2/2\pi)^2]^{1/2} \\ K_0 &= [(2\pi v_F - g_2)/(2\pi v_F + g_2)]^{1/2} \\ \gamma_0 &= \tfrac{1}{4}(K_0 + K_0^{-1} - 2) \end{aligned} \tag{3.10}$$

where these quantities have been taken at $p = 0$ and we have set $g_4(0) = 0$. The integrand in (3.9) has a branch cut in each variable and a pole at $\alpha + \mathrm{i}(a_F s + b_F s') = 0$ whose location depends on the other variable.

In the approximation of constant velocity v_0, v_F does not appear, $a_F = 1$ and $b_F = 0$, and the integral over s' decouples. This is the problem considered by Luther and Peschel [36], who evaluated that $\rho(q,\omega)$ approximately for small q and ω, but $\rho_r(q,\omega)$ can be evaluated without further approximation as

$$\rho_r(q,\omega) = \frac{\Lambda}{2v_0 \Gamma^2(\gamma_0)} \theta(\omega + rv_0 q)\theta(\omega - rv_0 q)\gamma\left(\gamma_0, \frac{\Lambda}{2v_0}(\omega + v_0 rq)\right) \times \left(\frac{\Lambda}{2v_0}(\omega - v_0 rq)\right)^{\gamma_0 - 1} \exp\left(-\frac{\Lambda}{2v_0}(\omega - v_0 rq)\right) + \begin{pmatrix} \omega \to -\omega \\ q \to -q \end{pmatrix} \quad \text{for } \gamma_0 \neq 0 \tag{3.11a}$$

$$\rho_r(q,\omega) = \delta(\omega - v_0 rq) \qquad \text{for } \gamma_0 = 0 \tag{3.11b}$$

where $\gamma(\alpha, x)$ is the incomplete gamma function.

Our regions of non-vanishing spectral weight and the exponents of divergence agree with Luther and Peschel. Unlike Luther and Peschel [36], who find a decay as ω^{-2} for large frequencies, our spectral function decreases exponentially. For $\gamma_0 = 0$, in equation (3.9) only the pole $s = \mathrm{i}\alpha$ survives and the s' integral then produces the δ-function.

This function has been described qualitatively before [29]. For $q > 0$, there is spectral weight at $\omega \geqslant v_0 q$ with an onset as $(\omega - v_0 q)^{\gamma_0 - 1}$, i.e. a divergence for $\gamma_0 < 1$, a cusp singularity for $1 \leqslant \gamma_0 \leqslant 2$, and a smooth onset for $\gamma_0 > 2$. At negative frequencies there is weight below $\omega = -v_0 q$ with an onset as $(-\omega - v_0 q)^{\gamma_0}$. This is appreciable only at small momenta $q\Lambda \ll 1$, and exponentially suppressed for larger q, cf equation (3.11). Apart from the transfer of this spectral weight from negative to positive frequencies as q is increased, the positive frequency part is scale-invariant and disperses with $v_0 q$. For $q = 0$, i.e. $k = k_F$, the divergence changes and $\rho(0, \omega) \sim |\omega|^{2\gamma_0 - 1}$. These features are illustrated in figures 1–3. Figure 1 displays $\rho(0, \omega)$ for various values of $\alpha = 2\gamma_0$. The change from a divergence to a cusp singularity is obvious. Here and in the following, we have determined v_0 from α via equation (3.10) and we have chosen as units $v_F = 1$, $\Lambda = 1$. Figure 2 displays the asymmetric shape of $\rho(q, \omega)$ for finite q, here $q = 0.1$, and its evolution with α. The asymptotic behaviour of equation (3.11*a*) is not always apparent here, especially for the larger α. In fact, for $\alpha > 1$, significant spectral weight resides at negative frequencies, which is taken out of the positive frequency part somewhat behind the onset. This is obvious from the inset of figure 2 where the region $\omega \simeq v_0 q$ for $\alpha = 3$ has been blown up. Although not apparent on the full scale, the asymptotic prediction $\rho \sim (\omega - v_0 q)^{1/2}$ of equation (3.11*a*) is satisfied. At higher q, the spectral weight at negative frequencies decreases exponentially, changing somewhat the shape of the $\omega > 0$ part. This is seen in figure 3 where $q = 0.5$ and we only show the positive frequency part. Also the asymptotic behaviour for $\omega \simeq v_0 q$ is much more prominent, confirming that it is masked by transfers of spectral weight to $\omega < 0$ as $q \to 0$. Figure 4 finally shows the dispersion with q of the spectral function for $\alpha = 0.125$. The large values of α in figures 1–3 may appear of purely academic interest in view of the limitation $\alpha \leqslant 1/8$ for the Hubbard model. However, experiments [24, 28] do suggest values of α in excess of unity and it is important to study the evolution of $\rho(q, \omega)$ in this regime. We only show figures for $q \geqslant 0$, where $\omega < 0$ corresponds to photoemission and $\omega > 0$ to inverse photoemission. For $q < 0$, the spectral function is obtained by simple reflection at $\omega = 0$ from that at $q > 0$.

The spectral weight at positive frequencies corresponds to the creation of a particle above the Fermi sea $\langle c_{k_F+q,s}(t) c^+_{k_F+q,s}(0)\rangle$ with $q > 0$ while the response at negative frequencies comes from the hole creation above the Fermi sea $\langle c^+_{k_F+q,s}(0) c_{k_F+q,s}(t)\rangle$. This process is not allowed in a free Fermi gas but occurs here due to the finite number of particles excited above k_F in the ground state by the interaction g_2. This is most easily seen from the momentum distribution function $n(k)$, equation (3.5), which is finite for $q > 0$. The asymmetry of the spectral response is due to the small number of particles excited above k_F in the ground state. The spread in spectral weight is caused by the g_2 interaction allowing an incoming particle to evaporate an arbitrary number of particle–hole pairs on the opposite branch (as in the x-ray edge problem).

The relevant processes are depicted schematically in figure 5. Consider the Lehmann representation

$$\rho(k, \omega) = \theta(\omega)\rho^+(k, \omega) + \theta(-\omega)\rho^-(k, -\omega) \tag{3.12a}$$

with

$$\rho^+(k, \omega) = 2\pi \sum_n |\langle \psi_n^{N+1} | c_k^+ | \psi_0^N \rangle|^2 \delta(\varepsilon_n^{N+1} - \omega) \tag{3.12b}$$

$$\rho^-(k, \omega) = 2\pi \sum_n |\langle \psi_n^{N-1} | c_k | \psi_0^N \rangle|^2 \delta(\varepsilon_n^{N-1} - \omega) \tag{3.12c}$$

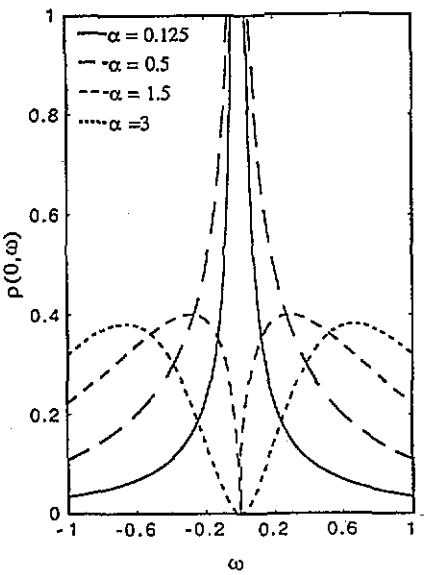

Figure 1. Spectral function $\rho(0,\omega)$ at the Fermi wavevector for different values of α. This plot is equally valid for the spinless and spinful Luttinger liquid.

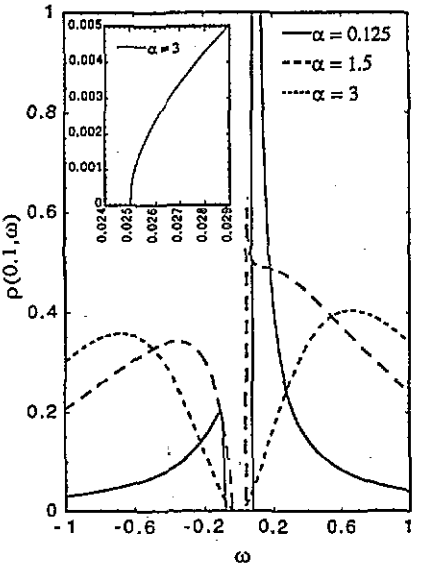

Figure 2. Spectral function $\rho(q,\omega)$ of the spinless Luttinger liquid for $q = 0.1$ and various α. Here and in all following figures, units are chosen as $\Lambda = 1$ and $v_F = 1$. The inset shows the asymptotic behaviour close to the onset of spectral weight for $\alpha = 3$ to be in agreement with the prediction of equation (3.11), although this is not apparent on the scale of the main figure. This figure, as well as figures 3 and 4, use the approximation of constant renormalized charge velocity. The relation between the α values in the figures and the velocities is that for the Luttinger *model* and the procedure for conversion is explained in the *text*.

in obvious notation [37]. In figure 5(a) in step (1) an electron is injected into the system with wavevector $k_F + q$. H_2, equation (2.6b), generates a particle–hole excitation with $p > 0$ on both sides of the Fermi surface, giving an energy

$$\varepsilon^{N+1} = vq + 2vp \geqslant vq \tag{3.13}$$

after step (2). In figure 5(b), the particle–hole excitations are created first in order to have electrons above k_F. In step (2), one of these electrons is ejected, i.e. a hole is added to the system. Then

$$\varepsilon^{N-1} = 2vp - vq \geqslant vq \tag{3.14}$$

since the particles excited in (1) must come from below the Fermi surface, i.e. $p \geqslant q$. This produces spectral weight for $\omega < -vq$ since we have $\rho^-(k,-\omega)$ in (3.12a). Similarly, the injected particle in figure 5(a) can be relaxed by a particle–hole excitation with $p < 0$ if one had excited particles in the system before the arrival of the test particle. These processes also contribute to the part at $\omega > v_0 q$.

The main shortcoming of equation (3.11) is the inadequate description of the higher-energy properties of the model. It seems natural to expect the spectral response to be

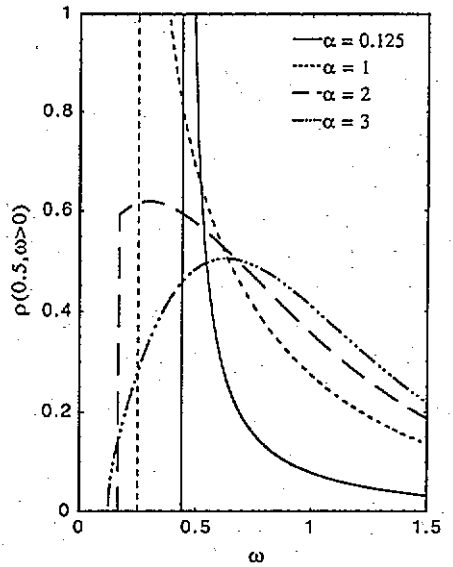

Figure 3. Spectral function $\rho(q,\omega)$ of the spinless Luttinger liquid for various α. Only the positive frequency part is displayed.

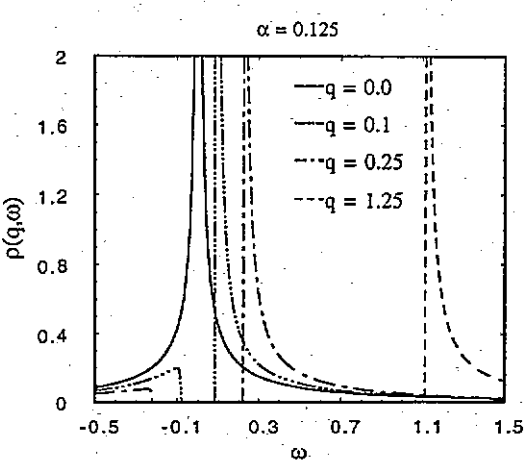

Figure 4. Dispersion of the spectral function $\rho(q,\omega)$ for $\alpha = 0.125$ with q.

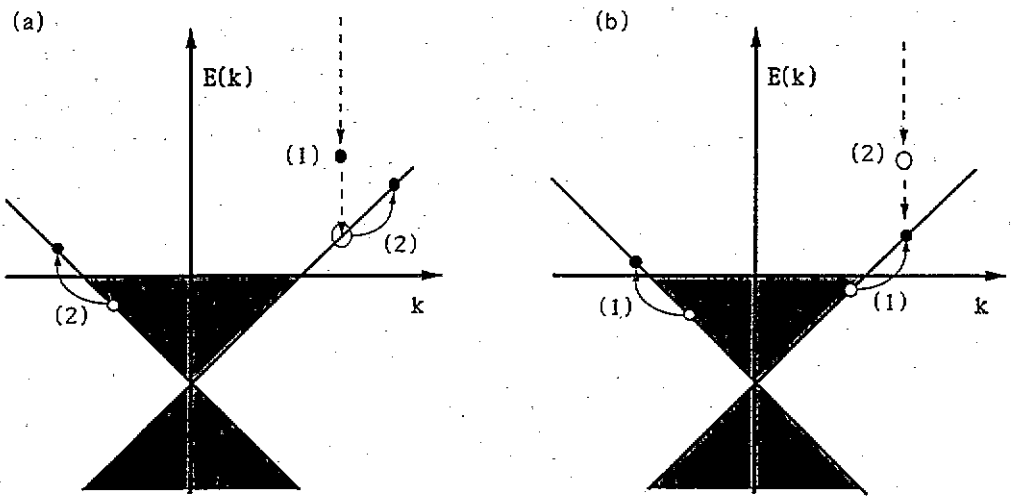

Figure 5. Sketch of the mechanism for the generation of spectral weight by hybridization of the Fermi surfaces via g_2 at positive frequencies (*a*) and negative frequencies (*b*), cf text. Event (1) occurs before event (2).

determined by $v_F q$ at values of $q \gg \Lambda^{-1}$ instead of $v_0 q$ in (3.11), and naively one would expect $\rho(q,\omega)$ to become a δ-function as $q \to \infty$ and interactions become unimportant. To remedy this problem, one must treat correctly the short-range properties of the model and prefer the Green function (2.13) to the approximate one (2.15), simplified, of course, to spinless fermions. We then have to evaluate the full integral (3.9). The $\rho(q,\omega)$ can be decomposed into three terms:

$$\rho_1(q,\omega) = \frac{1}{8\pi^2 v_0 \Lambda}\int_{-\infty}^{\infty} ds\exp(is\Omega_1)\left(1+\frac{is}{\Lambda}\right)^{-1-\gamma_0}\int_{-\infty}^{\infty} ds'\exp(is'\Omega_2)\left(1+\frac{is'}{\Lambda}\right)^{-\gamma_0}$$
$$+(\Omega_1\to-\Omega_1,\Omega_2\to-\Omega_2)$$
$$=\frac{\Lambda}{2v_0}\frac{\theta(\Omega_1)\theta(\Omega_2)}{\Gamma(\gamma_0)\Gamma(1+\gamma_0)}(\Lambda\Omega_1)^{\gamma_0}(\Lambda\Omega_2)^{\gamma_0-1}\exp[-\Lambda(\Omega_1+\Omega_2)]$$
$$+(\Omega_1\to-\Omega_1,\Omega_2\to-\Omega_2). \tag{3.15}$$

Here the pole in equation (2.4) is cancelled by the vanishing residue $i(a_F s + b_F s') \times (\ldots)$ in the numerator and only the branch cuts contribute. There is a finite residue of the pole from the remaining term in the numerator

$$\rho_2(q,\omega) = \frac{\theta(\Omega_2)}{4\pi v_0 b_F}\int_{-\infty}^{\infty} ds\exp\{is[\Omega_1-(a_F/b_F)\Omega_2]\}\left(1+\frac{is}{\Lambda}\right)^{-1-\gamma_0}\left(1-i\frac{a_F s}{b_F\Lambda}\right)^{-\gamma_0}$$
$$+(\Omega_1\to-\Omega_1,\Omega_2\to-\Omega_2). \tag{3.16}$$

Finally there is the contribution from the integral along the s' cut:

$$\rho_3(q,\omega) = \frac{-\theta(\Omega_2)}{4\pi v_0 b_F\Gamma(\gamma_0)}(\Lambda\Omega_2)^{(\gamma_0-1)/2}\exp(-\Lambda\Omega_2/2)$$
$$\times\int_{-\infty}^{\infty} ds\exp\{is[\Omega_1-(a_F/b_F)\Omega_2]\}\left(1+\frac{is}{\Lambda}\right)^{-1-\gamma_0}$$
$$\times\left(1-i\frac{a_F s}{b_F\Lambda}\right)^{-(\gamma_0+1)/2} W_{(\gamma_0-1)/2,-\gamma_0/2}\left[\Lambda\Omega_2\left(1-i\frac{a_F s}{b_F\Lambda}\right)\right]$$
$$+(\Omega_1\to-\Omega_1,\Omega_2\to-\Omega_2) \tag{3.17}$$

where $W_{\lambda,\mu}(z)$ is Whittaker's function [38]. This function can be represented as a sum of two confluent hypergeometric functions [39]†, one of which reduces to an exponential and cancels $\rho_2(q,\omega)$. For the remainder of $\rho_3(q,\omega)$, we use an integral representation [40] for the confluent hypergeometric function to obtain

$$\rho_2(q,\omega)+\rho_3(q,\omega) = \frac{\Lambda\theta(\Omega_2)}{2v_0 b_F\Gamma(\gamma_0)\Gamma(1+\gamma_0)}(\Lambda\Omega_2)^{\gamma_0}\exp[-\Lambda(\Omega_1+\Omega_2)]$$
$$\times\int_0^1 dt\,\theta\left(\Omega_1-\frac{a_F}{b_F}\Omega_2 t\right)\left[\Lambda\left(\Omega_1-\frac{a_F}{b_F}\Omega_2 t\right)\right]^{\gamma_0}(1-t)^{\gamma_0-1}$$
$$\times\exp[\Lambda\Omega_2(1+a_F/b_F)t]+(\Omega_1\to-\Omega_1,\Omega_2\to-\Omega_2)$$
$$=\frac{\Lambda\theta(\Omega_2)(\Lambda\Omega_2)^{\gamma_0}\exp[-\Lambda(\Omega_1+\Omega_2)]}{2v_0 b_F\Gamma(\gamma_0)\Gamma(1+\gamma_0)}\times\left[\frac{1}{\gamma_0}\theta\left(\Omega_1-\frac{a_F}{b_F}\Omega_2\right)(\Lambda\Omega_1)^{\gamma_0}\right.$$
$$\times\phi_1\left(1,-\gamma_0,1+\gamma_0;\frac{a_F\Omega_2}{b_F\Omega_1};\Lambda\Omega_2\left(1+\frac{a_F}{b_F}\right)\right)$$
$$+\frac{1}{1+\gamma_0}\theta(\Omega_1)\theta\left(\frac{a_F}{b_F}\Omega_2-\Omega_1\right)\left(\frac{b_F\Omega_1}{a_F\Omega_2}\right)(\Lambda\Omega_1)^{\gamma_0}$$
$$\left.\times\phi_1\left(1,1-\gamma_0,2+\gamma_0;\frac{b_F\Omega_1}{a_F\Omega_2};\Lambda\Omega_1\left(1+\frac{a_F}{b_F}\right)\right)\right]$$
$$+(\Omega_1\to-\Omega_1,\Omega_2\to-\Omega_2). \tag{3.18}$$

† Formulae in Gradshteyn and Ryzhik [39] will be abbreviated as GR $x \cdot yyy, z$.

GR 3.385 has been used in the last equality and $\phi_1(a,b,c;x;y)$ is the confluent hypergeometric function of two variables, GR 9.26.

The part $\rho_1(q,\omega)$ is quite similar in structure to the spectral function (3.11) and, in fact, is the dominant contribution for small q with an onset at positive frequencies at $v_0 q$ with exponent $\gamma_0 - 1$ and a weaker singularity (exponent γ_0) at $\omega < -v_0 q$. The important difference lies in the exponential factor $\exp(-\Lambda\omega/v_0)$ strongly suppressing contributions from this term for $q\Lambda \gtrsim 1$.

We turn to equation (3.18). The first term in the large square brackets contributes for $v_0 q < \omega < v_F q$ (if $q > 0$) with an onset as $(\omega - v_0 q)^{\gamma_0}$, i.e. a weaker singularity than $\rho_1(q,\omega)$ for small q, and peaks at $v_F q$. The second decays from $\omega = v_F q$ on towards higher ω, implying a maximum at $\omega = v_F q$. Since standard references [38, 39] do not give much information on $\phi_1(a,b,c;x;y)$ we prefer a numerical evaluation of the integral in equation (3.18) for generating the following plots.

Figure 6 displays the positive frequency parts of $\rho(q,\omega)$ for $\alpha = 0.125$ and various q. Generically, there is a double-peak structure with the two features located at $\omega = v_0 q$ and $\omega = v_F q$. Figure 6(*a*) shows that, at small q, all spectral weight resides in the divergence at $v_0 q$. At large q the peak at $v_F q$ dominates. Figures 6(*b*) and (*c*) decompose the total spectral function into $\rho_1(q,\omega)$, equation (3.15), and $\rho_2(q,\omega)$, standing for equation (3.18). The $\rho_1(q,\omega)$ has a power-law divergence at $\omega = v_0 q$ whose amplitude is, however, suppressed as $\exp[(\omega + v_0 q)\Lambda/2v_0]$ as q is increased. On the high-frequency side of ρ_1 develops a contribution from ρ_2, which is peaked at $\omega = v_F q$, i.e. the unrenormalized dispersion. It is apparent that as q is increased spectral weight is transferred from the narrow peak at $\omega = v_0 q$ into the broad bump between $v_0 q$ and $v_F q$ while the response beyond $v_F q$ is very weak. This peak sharpens as q increases but one does not recover a $\delta(\omega - v_F q)$ signal as $q \to \infty$; instead one forms an asymmetric structure at $v_F q$ with a more gradual rise from lower frequencies and an extremely sharp drop towards higher frequencies.

One may be surprised to find that spectral weight is simply transferred, like in communicating tubes, between features located at $v_0 q$ (i.e. the $q \to 0$ limit of the dispersion) and $v_F q$ (i.e. its $q \to \infty$ limit) while the renormalized velocity $v_0(p)$ of the bosons is p-dependent through $g_2(p)$. It is tempting to associate the loss of any p dependence interpolating between $v_0 q$ and $v_F q$ to our evaluation of the Green function, equation (2.13), to logarithmic accuracy (in the exponentials) where the results are independent of the explicit p dependence of $g_2(p)$. On the other hand, an evaluation beyond logarithmic terms using very special p dependences of g_2 produces a similar double-peak response [41], suggesting that there is little contribution to the fermionic properties from such non-universal terms.

Figure 7 finally shows the positive frequency part of $\rho(q,\omega)$ for $\alpha = 0.5$ (*a*) and $\alpha = 3$ (*b*). The bigger difference $v_F - v_0$ for larger α makes the double-peak structure in ρ and the shift of spectral weight with q between both peaks already quite apparent at $\alpha = 0.5$. The evolution with α is also very interesting. As α increases to produce a cusp-like (or even flat) onset, e.g. $\alpha = 3$, the maximum of spectral weight is pushed up a finite distance from the onset $v_0 q$. For $q < 1$, the maximum in figure 7(*b*) is at $\omega \sim 0.5$ independent of q so long as $q < 1$. Only for $q \gg 1$, when the $v_F q$ peak dominates the spectrum, does the maximum start dispersing.

3.1.2. One-branch Luttinger model. The second toy problem we consider is the spin-1/2 one-branch Luttinger liquid, $g_{2\rho} = g_{2\sigma} = 0$. For $g_{4\perp} \neq 0$, $v_\rho \neq v_\sigma$ and this model exhibits charge–spin separation. The correlation function exponents $K_\nu = 1$ are, however, those of free fermions. The Green function is directly obtained from equations (2.13) or (2.15) by setting $\gamma_\nu = 0$. In the approximation (2.15) where only the renormalized velocities appear,

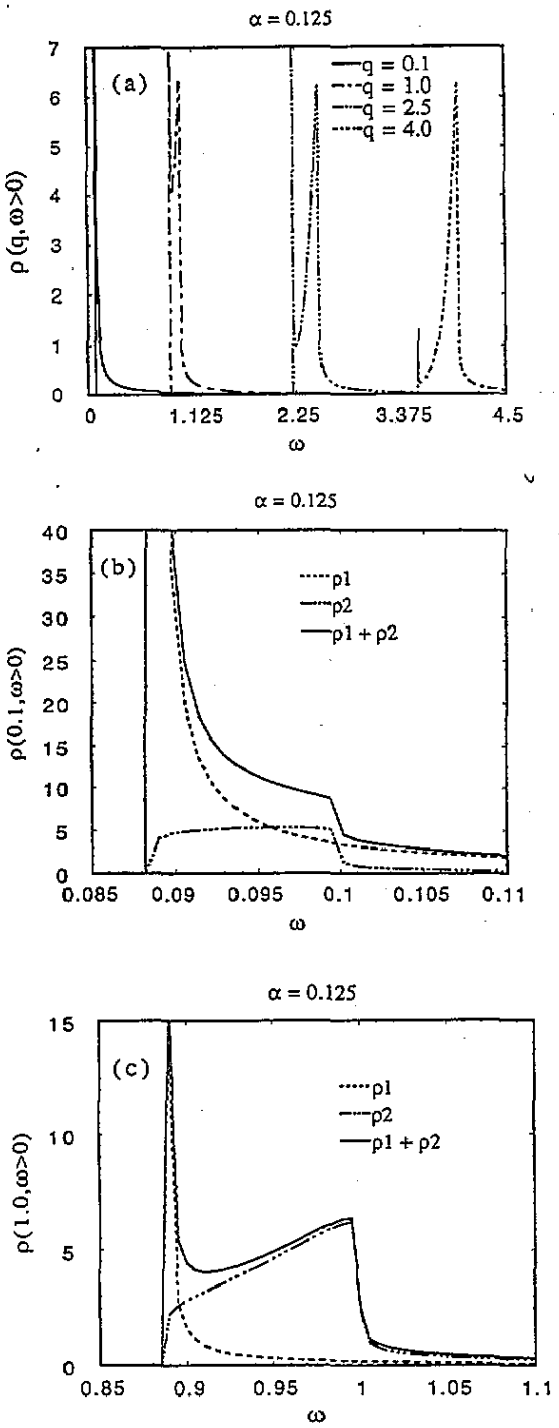

Figure 6. (*a*) Dispersion of the positive frequency part of the spectral function $\rho(q, \omega)$ for $\alpha = 0.125$ when the p dependence of the renormalized velocity is accounted for. (*b*) and (*c*) Decomposition of the total spectral function into the contributions of equations (3.15) and (3.18) and the transfer of spectral weight from the divergence at $v_0 q$ into the peak at $v_F q$ as q is increased.

the spectral function is

$$\rho(q,\omega) = \frac{\theta(\omega - v_\sigma rq)\theta(v_\rho rq - \omega) + \theta(v_\sigma rq - \omega)\theta(\omega - v_\rho rq)}{\pi(|\omega - v_\sigma rq||\omega - v_\rho rq|)^{1/2}} \tag{3.19}$$

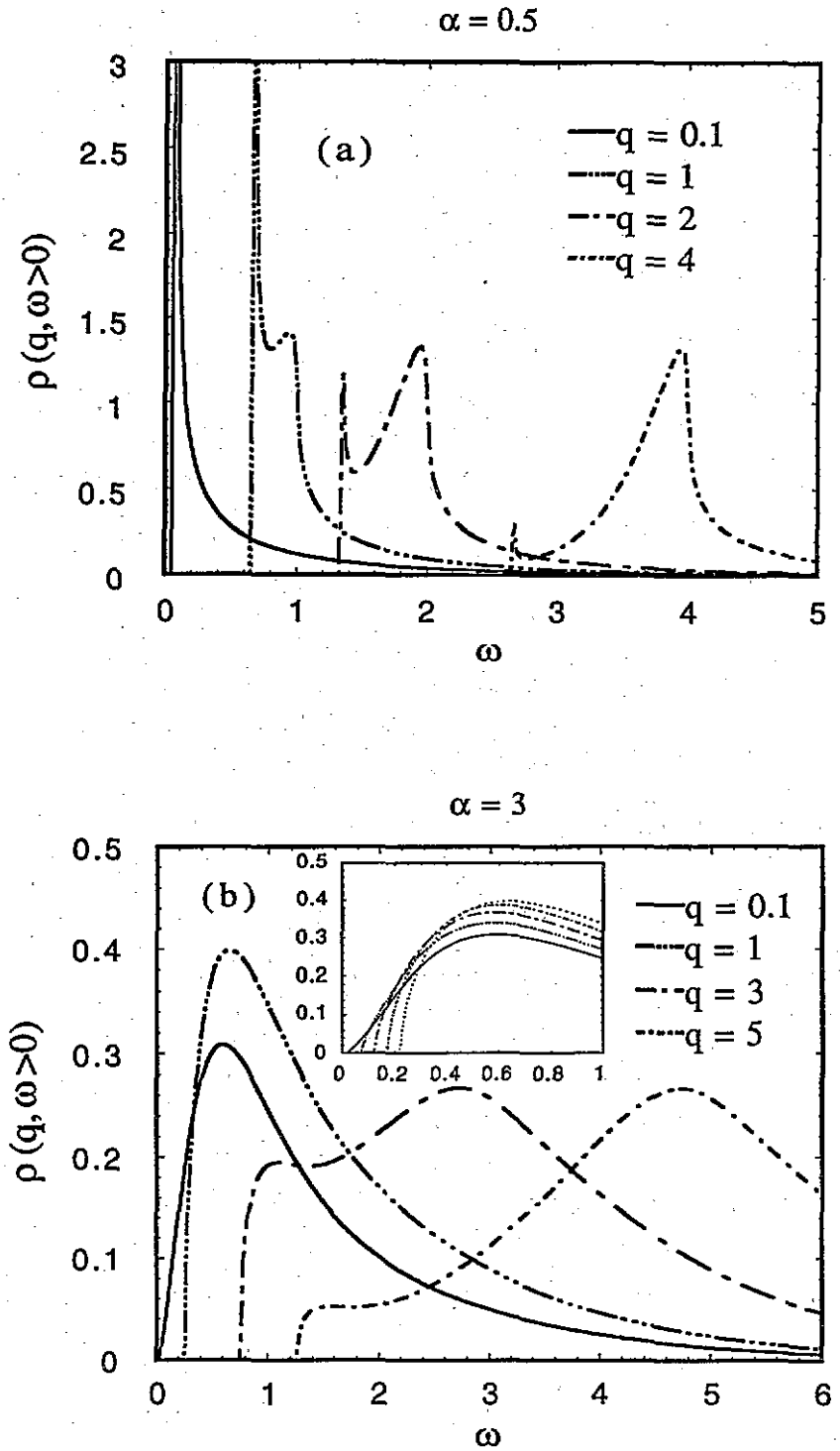

Figure 7. Dispersion of the spectral function $\rho(q, \omega)$ for $\alpha = 0.5$ (*a*) and $\alpha = 3$ (*b*). The respective contributions of equations (3.15) and (3.18) are apparent here. The inset in (*b*) demonstrates that, for $\alpha = 3$, the maximum does not change position as long as $q < 1$; represented are values of q from 0.1 (full curve) to 0.9 (dotted curve) in steps of 0.2.

which has been discussed previously [6, 29] and is not replotted here.

A calculation including the crossover to the correct high-(q,ω) limit is, however, possible starting from (2.13). It closely parallels the one outlined above for spinless fermions, and we obtain

$$\rho(q,\omega)=\rho_1(q,\omega)+\rho_2(q,\omega)$$

with

$$\rho_1(q,\omega)=\theta(\Omega_3)\theta(\Omega_4)\frac{\Lambda}{\pi|v_\rho-v_\sigma|}\frac{\exp[-\Lambda(\Omega_3+\Omega_4)]}{(|\Lambda\Omega_3||\Lambda\Omega_4|)^{1/2}}+(\Omega_3\to\Omega_3,\Omega_4\to-\Omega_4) \quad (3.20)$$

and

$$\begin{aligned}\rho_2(q,\omega)=\theta(\Omega_3)\theta(\Omega_4)&\frac{2}{\pi^{1/2}c_F|v_\rho-v_\sigma|}\left(\frac{\Omega_4}{\Omega_3}\right)^{1/2}\\&\times\left[\theta\left(\Omega_3-\frac{c_F}{d_F}\Omega_4\right)\phi_1\left(1,\frac{1}{2},\frac{3}{2};\frac{c_F\Omega_4}{d_F\Omega_3};\Lambda\Omega_3\left(1+\frac{c_F}{d_F}\right)\right)\right.\\&\left.+\theta\left(\frac{c_F}{d_F}\Omega_4-\Omega_3\right)\frac{d_F\Omega_3}{c_F\Omega_4}\phi_1\left(1,\frac{1}{2},\frac{3}{2};\frac{d_F\Omega_3}{c_F\Omega_4};\Lambda\Omega_3\left(1+\frac{c_F}{d_F}\right)\right)\right]\\&+(\Omega_3\to-\Omega_3,\Omega_4\to-\Omega_4).\end{aligned} \quad (3.21)$$

We have defined

$$\begin{aligned}&\Omega_3=(\omega-v_\rho rq)/(v_\rho-v_\sigma) \qquad \Omega_4=(v_\rho rq-\omega)/(v_\rho-v_\sigma)\\&c_F=(v_F-v_\sigma)/(v_\rho-v_\sigma) \qquad d_F=(v_\rho-v_F)/(v_\rho-v_\sigma).\end{aligned} \quad (3.22)$$

For the model *defined* by equation (2.1) $c_F=d_F=1/2$, but in a more general situation [32, 33] they may be different. Whenever an ordering of v_ρ and v_σ was necessary, we have chosen $v_\rho>v_\sigma$ corresponding to repulsive interactions (we shall make the same choice for the full problem below). For attractive interactions, the role of v_ρ and v_σ is reversed. The $\rho_1(q,\omega)$ is quite similar to the earlier result (3.19) apart from an additional exponential factor suppressing its contribution at high q. More interesting is, in fact, $\rho_2(q,\omega)$. This function behaves like $(\omega-v_\nu q)^{1/2}$ close to the borders of the region of spectral response but exhibits a logarithmic singularity at $\omega=v_F q$ in its centre. In figure 8(a) we show $\rho(q,\omega)$ for $q=0.5$ and $g_{4\perp}=0.5$ and its decomposition into ρ_1 and ρ_2. For the same $g_{4\perp}$, figure 8(b) displays the dispersion of $\rho(q,\omega)$ with q. It is apparent that, in a way similar to the spinless fermion case, spectral weight is transferred from the square-root divergences into the log singularity as q is increased. For $q=5$, the square-root divergence is no longer visible and the singularity at $v_F q$ contains the full spectral weight.

The inverse square-root singularities at the spin and charge fluctuation dispersions collapse into a $\delta(\omega)$ peak as $q\to 0$. This implies a momentum distribution function

$$n(k)=\theta(k_F-k) \quad (3.23)$$

in agreement with Luttinger's theorem [42] and would suggest a Fermi-liquid picture. It is clear, however, from the dispersion of the shape of the spectral function with q, that the physical picture must be radically different and that the notion of a quasiparticle does not make sense. The incident electron decays into a multiple charge (resp. spin) carrying particle–hole fluctuation on the same side of the Fermi surface. There is no spectral weight at negative energies because there are no particles present in the ground state above k_F.

The preceding discussion demonstrates that $n(k)$, and, more generally, any physical quantity depending on k or ω alone, is insensitive to the effects of charge–spin separation and is dominated by the power laws generated by the anomalous dimensions of the fermion operators. Charge–spin separation is visible only in the full q- and ω-dependent dynamical correlation functions. Quantities depending on q or ω alone can only probe the power-law correlations.

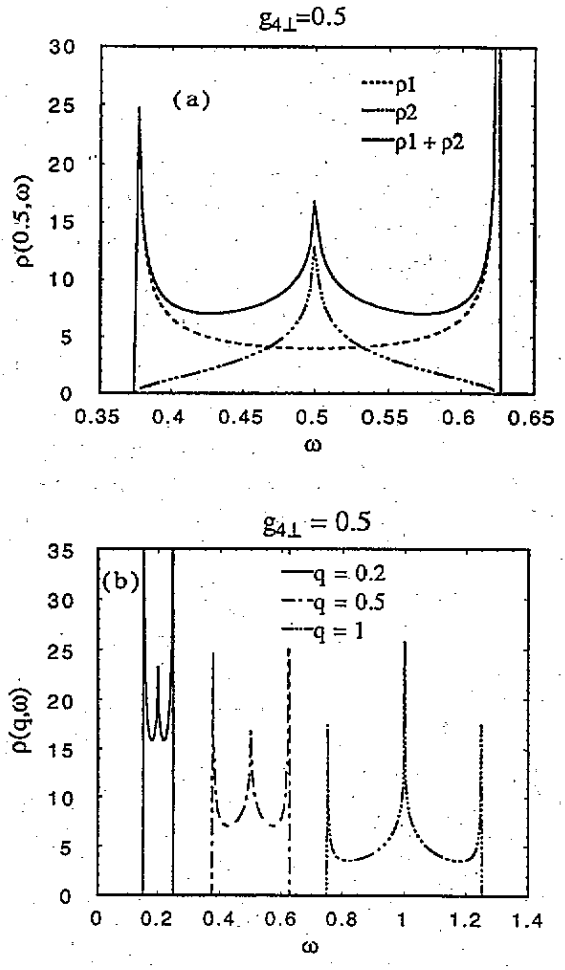

Figure 8. Spectral function for the one-branch Luttinger liquid. (*a*) Decomposition of $\rho(0.5,\omega)$ into the contributions of equations (3.20), giving inverse square-root divergences at the edges, and (3.21), producing a logarithmic singularity at the centre. (*b*) The dispersion with q and the transfer of spectral weight between the two features.

3.1.3. Spinful Luttinger model. We are now in a position to discuss the spectral properties of the spinful Luttinger liquid, described by the Green function (2.13). This problem involves three velocities (v_F, v_ρ and v_σ) and is extremely difficult to solve. We shall therefore discuss the approximate Green function (2.15) where v_F does not appear and v_ρ and v_σ govern the dynamics of the charge and spin fluctuations over all energy scales.

From the previous discussion, we would expect power-law singularities at $\omega = \pm v_\nu q$ and a region of zero spectral weight between $\pm v_\sigma q$ (for $v_\sigma < v_\rho$). The latter is determined by the analytic properties of $G(x,t)$, which become most prominent upon introducing separate coordinates for right- and left-moving fluctuations of the type with the smallest velocity (here spin fluctuations):

$$s = v_\sigma t - rx \qquad s' = v_\sigma t + rx \tag{3.24}$$

producing

$$\rho_r(qr,\omega) = \frac{\Lambda^{2\gamma_r}}{8\pi^2 v_\sigma}\int_{-\infty}^{\infty} ds \int_{-\infty}^{\infty} ds' \exp(i\Omega_1 s)\exp(i\Omega_2 s')$$
$$\times[(\alpha+is)^{1/2}(\Lambda+is)^{-\gamma_\sigma}(\Lambda+is')^{-\gamma_\sigma}(\alpha+ia_\rho s+ib_\rho s')^{-1/2}(\Lambda+ia_\rho s+ib_\rho s')^{-\gamma_\rho}$$
$$\times(\Lambda+ia_\rho s'+ib_\rho s)^{-\gamma_\rho}+(s\to -s, s'\to -s')] \tag{3.25}$$

with the definitions

$$\Omega_1 = \omega/(2v_\sigma) + rq_r/2 \qquad \Omega_2 = \omega/(2v_\sigma) - rq_r/2$$
$$a_\rho = (v_\rho + v_\sigma)/(2v_\sigma) \qquad b_\rho = (v_\rho - v_\sigma)/(2v_\sigma). \tag{3.26}$$

Both the s and s' integrands have non-analyticities (branch cuts) only in the complex upper half-plane, implying that spectral response is limited to $\Omega_1 > 0$ and $\Omega_2 > 0$, i.e. $\omega > v_\sigma q$. The term produced by inverting s and s' yields a contribution only for $\omega < -v_\sigma q$. Also the asymptotic behaviour close to $\omega = \pm v_\sigma q$ is quite apparent: one has $\Omega_2 \simeq 0$, Ω_1 finite (resp. the opposite) and obtains from power counting

$$\rho_r(q, \omega \simeq v_\sigma q) \sim \theta(\omega - v_\sigma q)(\omega - v_\sigma q)^{2\gamma_\rho + \gamma_\sigma - 1/2}$$
$$\rho_r(q, \omega \simeq -v_\sigma q) \sim \theta(-\omega - v_\sigma q)(-\omega - v_\sigma q)^{2\gamma_\rho + \gamma_\sigma}. \tag{3.27}$$

The second line applies only for $\gamma_\sigma > 0$; for $\gamma_\sigma = 0$, spectral weight appears only at $\omega = -v_\rho q$ (keep s as above but use $s' = v_\rho t + rx$ to see this). The divergences at $\omega = \pm v_\rho q$ are best seen by going to new variables ξ and ξ' obtained from (3.19) by replacing $v_\sigma \to v_\rho$. Then we find

$$\rho_r(q, \omega \simeq v_\rho q) \sim |\omega - v_\rho q|^{\gamma_\rho + 2\gamma_\sigma - 1/2}$$
$$\rho_r(q, \omega \simeq -v_\rho q) \sim |\omega - v_\rho q|^{\gamma_\rho + 2\gamma_\sigma}. \tag{3.28}$$

These exponents agree with [30] and reduce, for $\gamma_\sigma = 0$ (spin-rotation invariance), to those given earlier [29]. Equations (3.27) and (3.28) are quite different from the proposal by Anderson and Ren [14]. Their function has the correct regions of spectral weight at positive frequencies, but they give an exponent $\alpha = 2\gamma_\rho$ instead of $2\gamma_\rho - 1/2$ for the onset at $\omega = v_\sigma q$ and completely miss the divergence at $v_\rho q$. Moreover their pole at $\omega = -v_\rho q$ turns into an $(-\omega - vq)^{\gamma_\rho}$ singularity here.

For $\gamma_\sigma = 0$, a full calculation of the spectral function is possible with one major approximation: some integrals become solvable only upon replacing α in (3.25) by the cut-off Λ. This will modify the spectral function at higher energies and wavevectors and thereby violate the sum rule (3.2). (Roughly speaking for fixed α, a factor $\exp(-|q|\Lambda)$ is introduced into the spectral function. This is best seen by comparing equation (3.11) to (3.15): applying in the present approximation to (3.11) will precisely produce (3.15)!). The results to be shown below are therefore restricted to very small values of q and ω where the approximation does not affect the results in an important way. The details of this calculation have meanwhile been published by my competitors [30] and I shall not reproduce them here.

Figure 9 shows the dispersion with q of the spectral function for $\alpha = 0.125$ (i.e. the α of the $U = \infty$ Hubbard model). As before we determined $g_{4\perp} = g_{2\perp} = g_{2\parallel}$ from α via K_ρ (equation (2.9)) putting $K_\sigma = 1$ (spin-rotation invariance) and injected them into equation (2.8). It is apparent that the spectral function carries features both from the spinless fermion function (synonymous with 'anomalous fermion dimensions') and from the one-branch problem (synonymous with 'charge–spin separation'). The picture is, however, far more complicated than a simple addition of these two problems and, to some extent, multiple crossovers can take place between regimes where one or the other feature is prominent.

If q is very small (say $q = 0.001$), on the scale of the figure, $\rho(q, \omega)$ resembles pretty much the spinless fermion function. The separation of spin and charge at positive frequencies is not resolved at the scale of the plot but can, of course, be visualized by using a different scale. There is also a negative frequency contribution of deceptively small

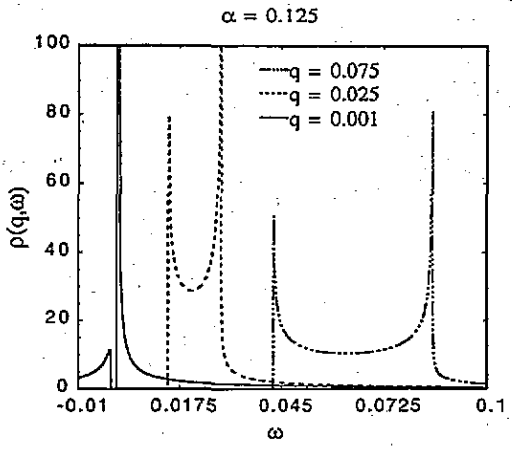

Figure 9. Dispersion of the spectral function $\rho(q,\omega)$ for the spinful Luttinger liquid for $\alpha = 0.125$, the value for the infinite-U Hubbard model. Notice the crossover, on the scale of the figure, of a spectral function similar to the spinless Luttinger liquid to one more reminiscent of the charge–spin separated one-branch problem.

amplitude whose cusp exponent 1/16 can hardly be distinguished from an edge discontinuity. As q is increased, charge and spin fluctuations respond at visibly different frequencies. Also apparent is the slightly larger exponent in the divergence at the charge excitation energy: the curve is slightly asymmetric and the peaks have larger amplitude at $v_\rho q$ as compared to $v_\sigma q$. Although the actual peak height is determined by the matching of $v_\nu q$ with the ω grid used in the plot, it is systematically higher at $v_\rho q$ for all q. As q increases, the weight at negative frequencies decreases exponentially and would hardly be visible in figure 9 for $q = 0.025$ and 0.075. It is also manifest from figure 9 that, at these small values of α and at not too small q, the spectral function is more similar to that of the one-branch problem than to those of the spinless fermions. The exponent at $v_\sigma q$ in figure 8 is $-3/8$ and at $v_\rho q - 7/16$ instead of $-1/2$ in the one-branch Luttinger liquid. In other words, for small correlation strength α, the charge–spin separation is the dominant feature in the single-particle properties of the Luttinger model (this may be different if v_σ and v_ρ are allowed to vary freely and when their difference is not too important). Thinking about experiments where a fixed resolution is imposed, figure 9 suggests that the double-peak structure characteristic of charge–spin separation is only resolved beyond a critical momentum.

Figure 10 shows the evolution of the spectral function as α is increased. For $k = k_F$ we have again $\rho(0,\omega) \sim |\omega|^{\alpha-1}$, and plots are quite similar to figure 1. As α is increased beyond unity, spectral weight is pushed far away from the Fermi surface. The same trend occurs at finite wavevector. Figure 10(a) displays the behaviour at rather small α for $q = 0.05$. The negative frequency part is very small and not shown. The spectral weight is mainly concentrated between $v_\sigma q$ and $v_\rho q$, and the difference in exponents of the two divergences is amplified as α increases. For $\alpha = 0.5$, one has an edge discontinuity at $v_\sigma q$ in agreement with (3.27), while close to $v_\rho q$, $\rho \sim |\omega - v_\rho q|^{-1/4}$. As one goes towards higher α, figure 10(b), the behaviour close to $v_\sigma q$ evolves into a cusp and finally into a flat onset, while close to $v_\rho q$, an upward cusp emerges for $\alpha > 1$, and precisely at $\alpha = 1$, one recovers a logarithmic divergence. For $\alpha > 1$, a maximum appears in $\rho(q,\omega)$ at high ω (0.3 to 1 in units of Λ/v_F) outside the range of figure 10(b). Moreover the contribution at $\omega < 0$ rises to become a sizable fraction of the one at $\omega > 0$. The differences to the Anderson–Ren predictions are readily visible. The evolution in figure 10 also demonstrates that the violation of the sum rule generated by the approximation above depends sensitively upon α.

Although we have not yet been able to solve the general problem including the crossover to the correct high-q limit of the dispersion, $\omega = v_F q$, predictions can be made based on the

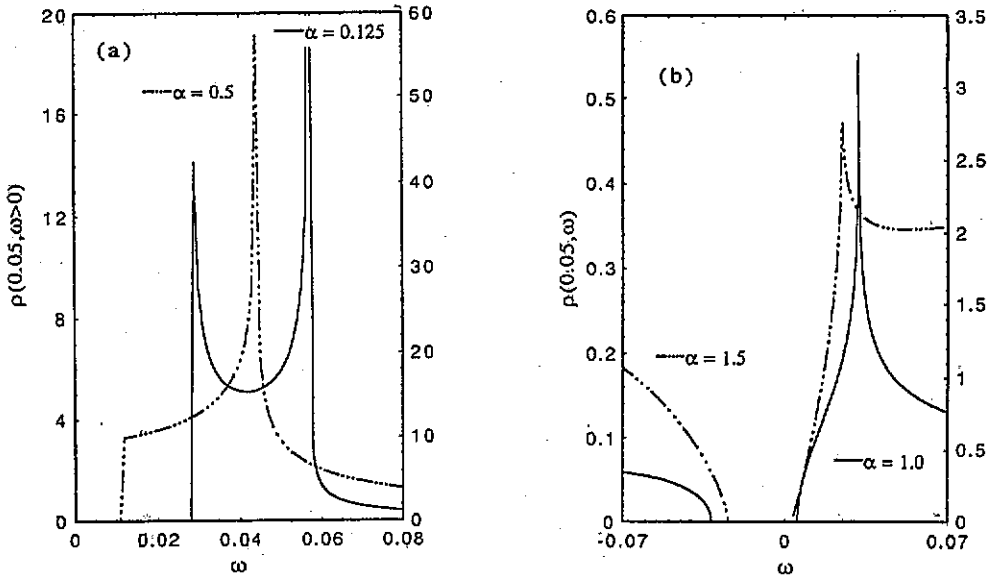

Figure 10. Evolution with correlation strength α of the spectral function $\rho(0.05, \omega)$ of the spinful Luttinger liquid. (*a*) 'Weak' correlation regime where charge–spin separation is dominant. (*b*) 'Strong' correlation regime where the anomalous fermion dimension effects are dominant. The α dependence of the sum-rule violation introduced by our approximation is also apparent.

present results and the understanding of this crossover we obtained in the spinless fermion and one-branch cases. Generically, we expect a third maximum in the spectral response at $v_F q$. This maximum will not be very pronounced at small q and small α but will grow out of the background as q and/or α are increased. If α is small, it will be located between $v_\sigma q$ and $v_\rho q$ and probably be quite similar to the one-branch Luttinger liquid. I do not, however, expect a true divergence at $v_F q$. As α increases, it should get more of the asymmetric edge-like structure of the spinless model and rather appear on the high-ω side of the $v_\rho q$ divergence. It is clear then that the signatures of charge–spin separation will fade away as one leaves the neighbourhood of the Fermi surface but one will not recover a δ-function as $q \to \infty$.

The mechanism of generation of spectral weight in the presence of charge–spin separation is sketched in figure 11. In step (1), a particle constituted by a charge and a spin part is absorbed by the system at wavevector q. The particle decomposes into a charge part with momentum $q - p$ and a spin part with momentum $q + p$, with $-q \leqslant p \leqslant q$. Following the reasoning of equations (3.12) and (3.13), the energy ε^{N+1} will become

$$\varepsilon_{\rm css}^{N+1} = \tfrac{1}{2}[v_\rho(q-p) + v_\sigma(q+p)] \tag{3.29a}$$

and be limited to

$$v_\sigma q \leqslant \varepsilon_{\rm css}^{N+1} \leqslant v_\rho q. \tag{3.29b}$$

This gives the spread of spectral weight due to charge–spin separation, i.e. all one has in the one-branch Luttinger liquid, equation (3.19). The g_4 scattering cannot change $\varepsilon_{\rm css}^{N+1}$. In step (2), particle–hole excitations in the charge channel (we assume $g_{2\rho} \neq 0$, $g_{2\sigma} = 0$) will boost the energy of the charge part of the particle similar to the spinless fermion problem, producing a spread in spectral weight beyond $\omega = v_\rho q$. The processes for generation of

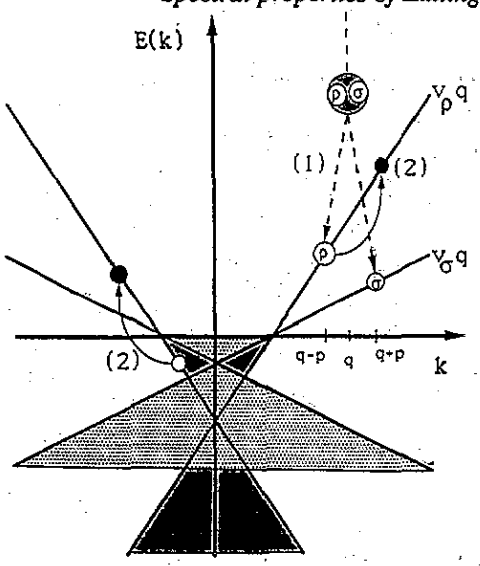

Figure 11. Sketch of the process at the origin of the spread in spectral weight in the presence of charge–spin separation. Event (1) (decomposition of an incoming particle–hole composite into its constituents) occurs before (2) and is the only one occurring in the one-branch problem. The spread of weight beyond $v_\rho q$ in (2) involves excitations on both branches.

weight at negative frequencies are then simply obtained by transforming the electron into a hole and inverting the order of steps (1) and (2).

Returning to the discussion of charge–spin separation, versus anomalous fermion dimensions, figure 10(a) demonstrates that charge–spin separation is the dominant feature at small α and that spectral weight is mainly concentrated between $v_\sigma q$ and $v_\rho q$. As the divergences disappear upon increasing α, an important transfer of spectral weight far away from the energies of the ejected (absorbed) particles (resp. their constituents) sets in and the aspects related to the anomalous fermion dimensions become prominent.

This suggests the following remark on the role of amplitude and range of electron–electron interactions. As long as the interactions are local (Hubbard model) the power-law corrections to correlation functions are surprisingly weak no matter what their amplitude is. In fact, the $U = \infty$ Hubbard model has $\alpha = 0.125$ and the influence of this exponent on the single-particle properties (not necessarily the many-particle correlation functions) is quite negligible. Dominant in the *dynamic* correlation functions is the charge–spin separation, which amounts to splitting a pole into a branch cut with singularities of roughly half the original degree of divergence at its ends—a dramatic modification of the low-energy physics! *Only a finite interaction range* allows the generation of really strong correlations in an intricate interplay of strength and range; and, ultimately, a Coulomb potential $V(q) \sim 1/q^2$ will always be in the strong-coupling limit no matter what its amplitude. In this case, strong modifications of the physics are generated by the correlations, and charge–spin separation plays a relatively minor role. Notice, however, that, in all these more realistic models, deviations from the asymptotic Luttinger-liquid spectral functions discussed here will occur for finite q and ω.

3.2. Real parts of Green functions

Although the real parts of the Green functions are of less immediate relevance for experiments, they are important in a variety of applications that use the interacting Luttinger model as a zeroth-order starting point in diagrammatic theories. An analytic calculation is not possible in general (except for the one-branch Luttinger liquid) and, for complete characterization, numerical procedures are required. A fairly detailed picture can also be composed from knowledge of the asymptotic behaviour of Re $G(q, \omega)$ in the vicinity of

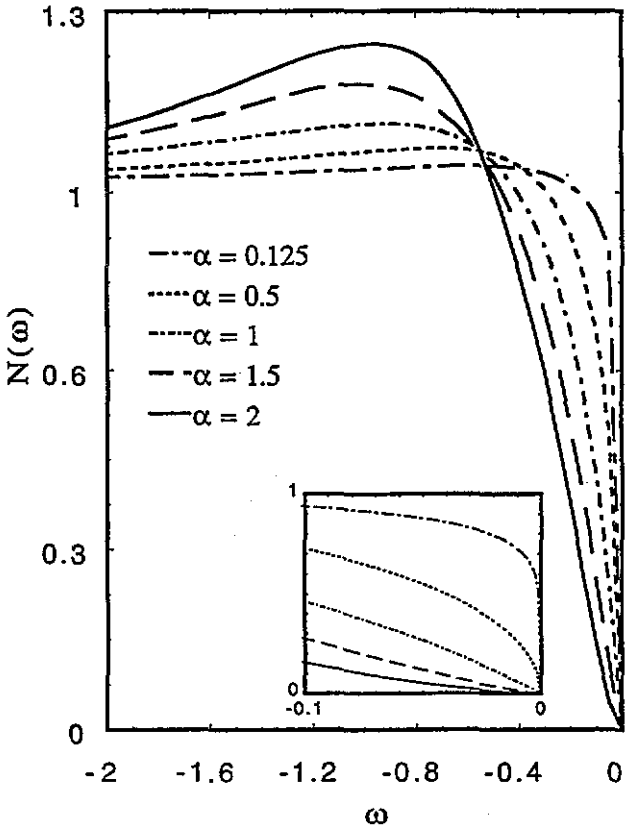

Figure 12. Energy-dependent density of states $N(\omega)$ of the Luttinger model for various α. The inset displays the asymptotic low-frequency behaviour close to the Fermi energy. Only the negative frequency part is shown.

the points $\omega = \pm v_\nu q$ where Im $G(q, \omega)$ behaves singularly. To this purpose we use the Kramers–Kronig relations

$$\mathrm{Re}\, G^{\mathrm{R}}(q, \omega) = \frac{1}{\pi} \mathrm{P} \int_{-\infty}^{\infty} \mathrm{d}\xi \, \frac{\mathrm{Im}\, G^{\mathrm{R}}(q, \xi)}{\xi - \omega} \tag{3.30}$$

where P denotes the principal value of the integral.

For the one-branch Luttinger liquid, equation (3.30) can be solved, and the real part is (here and below, we assume the branch $r = +$)

$$\mathrm{Re}\, G(q, \omega) = \frac{\theta(\omega - v_\rho q)\theta(\omega - v_\sigma q)}{[(\omega - v_\rho q)(\omega - v_\sigma q)]^{1/2}} - \frac{\theta(v_\sigma q - \omega)\theta(v_\rho q - \omega)}{[(v_\sigma q - \omega)(v_\rho q - \omega)]^{1/2}}. \tag{3.31}$$

Close to a one-sided power-law singularity

$$\rho(q, \omega) \sim \theta(\omega - vq)|\omega - vq|^{\gamma - 1}$$

$\mathrm{Re}\, G(q, \omega)$ varies like

$$\mathrm{Re}\, G(q, \omega) \sim \mathrm{sgn}(1 - \gamma)\, \mathrm{sgn}(\omega - vq)|\omega - vq|^{\gamma - 1} + \mathrm{const.} \tag{3.32}$$

If the spectral weight is to the other side of the divergence, say

$$\rho(q,\omega) = \theta(-\omega - vq)|-\omega - vq|^{\gamma-1}$$

one obtains

$$\mathrm{Re}\, G(q,\omega) \sim \mathrm{sgn}(1-\gamma)\,\mathrm{sgn}(\omega+vq)|\omega+vq|^{\gamma-1} + \text{const.} \tag{3.33}$$

Finally, it is obvious from (3.32) and (3.33) that close to a divergence from both sides

$$\rho(q,\omega) \sim |\omega - vq|^{\gamma-1}$$

$$\mathrm{Re}\, G(q,\omega) \sim \mathrm{sgn}(1-\gamma)\,\mathrm{sgn}(\omega-vq)|\omega-vq|^{\gamma-1} + \text{const.} \tag{3.34}$$

Finally, for $\gamma = 1$, i.e. a step in $\rho(q,\omega)$, the real part becomes

$$\mathrm{Re}\, G(q,\omega) \sim \ln|\omega - vq|. \tag{3.35}$$

For values of $\gamma < 1$, the divergence will dominate, but if γ increases beyond 1, one will find a cusp set off from zero by a finite value. The sign of the singular part changes when γ increases beyond 1, guaranteeing a smooth evolution of $\mathrm{Re}\, G(q,\omega)$ with γ.

4. Derived quantities: momentum distribution and density of states

Several physical properties can be derived directly from the Green function. Most important are the momentum distribution function

$$n(k) = -\mathrm{i}\int_{-\infty}^{\infty} \mathrm{d}x\, \mathrm{e}^{-\mathrm{i}kx} G_{r,s}(x,0^-) \tag{4.1}$$

where $G_{r,s}(x,0^-)$ is the time-ordered Green function, and the single-particle density of states

$$N(\omega) = \sum_r \int_{-\infty}^{\infty} \frac{\mathrm{d}q}{2\pi} \rho_r(q,\omega). \tag{4.2}$$

The asymptotic low-energy properties of these functions for the Luttinger model have been discussed earlier [1, 5, 35, 36, 43]; in view of the importance, in particular, of $N(\omega)$, for photoemission experiments, we shall recalculate them here and present some new results. Moreover, we want to use the full expression (2.13) in order to ensure the correct physics at higher energy scales.

We begin with $n(k)$. Inserting the $\langle\psi_{rs}^{+}\psi_{rs}\rangle$ part of (2.13) into (4.2), $n_{r,s}(k)$ for spin s and branch r is given by

$$\begin{aligned} n_{r,s}(k) &= \frac{-1}{2\pi}\int_{-\infty}^{\infty} \frac{\mathrm{d}x}{\alpha - \mathrm{i}rx}\left(\frac{\Lambda^2+x^2}{\Lambda^2}\right)^{-\gamma_\rho-\gamma_\sigma} \exp[-\mathrm{i}(k-rk_\mathrm{F})x] \\ &= \frac{1}{\pi}\,\mathrm{sgn}(k_\mathrm{F}-rk)\int_0^{\infty}\frac{\mathrm{d}x}{x}\left(\frac{\Lambda^2+x^2}{\Lambda^2}\right)^{-\gamma_\rho-\gamma_\sigma}\sin(|rk-k_\mathrm{F}|x) \end{aligned} \tag{4.3}$$

where the limit $\alpha \to 0$ has been performed in the second equality. Using GR 3.773, 1 one obtains finally

$$\begin{aligned} n_{r,s}(k) = \frac{1}{2\pi}\,\mathrm{sgn}(k_\mathrm{F}-rk)\Big[&B(\tfrac{1}{2},\gamma_\rho+\gamma_\sigma-\tfrac{1}{2}) \\ &\times \Lambda|rk-k_\mathrm{F}|\,{}_1F_2(\tfrac{1}{2};\tfrac{3}{2}-\gamma_\rho-\gamma_\sigma,\tfrac{3}{2};\tfrac{1}{4}\Lambda^2|rk-k_\mathrm{F}|^2) \\ &+\frac{\pi^{1/2}\Gamma(\frac{1}{2}-\gamma_\rho-\gamma_\sigma)}{\Gamma(1+\gamma_\rho+\gamma_\sigma)}\left(\frac{\Lambda}{2}|rk-k_\mathrm{F}|\right)^{2(\gamma_\rho+\gamma_\sigma)} \\ &\times {}_1F_2\,(\gamma_\rho+\gamma_\sigma;1+\gamma_\rho+\gamma_\sigma,\tfrac{1}{2}+\gamma_\rho+\gamma_\sigma;\tfrac{1}{4}\Lambda^2|rk-k_\mathrm{F}|)\Big] \end{aligned} \tag{4.4}$$

where $B(\alpha,\beta)$ is the beta function (GR 8.38) and ${}_1F_2(a;b,c;z)$ a generalized hypergeometric function (GR 9.14, 1). The asymptotic behaviour given in equation (3.6) is apparent because ${}_1F_2(a;b,c;0)=1$ and (4.4) then determines explicitly the constants C_1 and C_2 in (3.6).

The density of states

$$N(\omega)=\sum_r\int_{-\infty}^{\infty}\frac{\mathrm{d}q}{2\pi}\rho_r(q,\omega) \tag{4.5}$$

depends sensitively on the use of the Green function (2.13) or (2.15), i.e. the treatment of the high-energy physics outside the asymptotic regime $|\omega|\to 0$. For the Green function (2.15) we obtain for $\gamma_\sigma=0$

$$N(\omega)=\frac{1}{\pi(v_\rho v_\sigma)^{1/2}}\frac{\gamma(2\gamma_\rho,|\omega\Lambda/v_\rho|)}{\Gamma(2\gamma_\rho)}. \tag{4.6}$$

This function increases monotonically with $|\omega|$ and tends towards $1/\pi(v_\rho v_\sigma)^{1/2}$ as $|\omega|\to\infty$. This is different from and in general higher than the free-fermion density of states $1/\pi v_F$, indicating that the high-energy physics of the model has been altered by assuming constant velocities v_ν for charge and spin fluctuations. If the correct Green function (2.13) is used, one can take advantage of the pole in the first factor and evaluate $N(\omega)$ even for finite γ_σ as

$$\begin{aligned}N(\omega)=\frac{\Lambda^{2(\gamma_\rho+\gamma_\sigma)}v_\rho^{-2\gamma_\rho-1/2}v_\sigma^{-2\gamma_\sigma-1/2}}{\pi\Gamma(1+2\gamma_\rho+2\gamma_\sigma)}\Bigg[&\exp(-|\omega|\Lambda/v_\rho)|\omega|^{2(\gamma_\rho+\gamma_\sigma)}\\&\times{}_1F_1\left(\frac{1}{2}+2\gamma_\sigma,1+2\gamma_\rho+2\gamma_\sigma;\left(\frac{1}{v_\rho}-\frac{1}{v_\sigma}\right)\Lambda|\omega|\right)\\&+\frac{\Lambda}{v_F}\int_0^{|\omega|}\mathrm{d}\omega'\exp(-|\omega'|\Lambda/v_\rho)|\omega'|^{2(\gamma_\rho+\gamma_\sigma)}\\&\times{}_1F_1\left(\frac{1}{2}+2\gamma_\sigma,1+2\gamma_\rho+2\gamma_\sigma;\left(\frac{1}{v_\rho}-\frac{1}{v_\sigma}\right)\Lambda|\omega'|\right)\Bigg].\end{aligned} \tag{4.7}$$

An equivalent formula is contained in unpublished work by Schulz [44].

For low energies, the first term dominates and produces $N(\omega)\sim|\omega|^\alpha$, in agreement with the asymptotic results of Luther and Peschel [36] and Suzumura [35], while for high energies $N(\omega)$ tends to the free-particle density of states $1/\pi v_F$. $N(\omega)$ from equation (4.7) for $\gamma_\sigma=0$ is displayed in figure 12 where we used the procedure discussed above for generating the v_ν from α. It is apparent that the spectral weight lost in the pseudogap close to the Fermi surface reappears in a maximum at finite frequency. This suggests the existence of another sum rule for the Luttinger model translating a conservation of the total spectral weight of the model in the presence of interactions. In fact, Suzumura [35] has shown that

$$\int_0^\infty\mathrm{d}\omega\left(N(\omega)-\frac{1}{\pi v_F}\right)=0 \tag{4.8}$$

and our equation (4.7) obeys that rule. Upon close inspection, some curves in figure 12, in particular the one for $\alpha=0.125$, seem to violate this rule. There is, however, for small α another shallow minimum in $N(\omega)$ at higher energies (e.g. for $\alpha=0.125$ at $\omega\simeq 3.5$) as can be checked by examining the derivative $\mathrm{d}N(\omega)/\mathrm{d}\omega$. This minimum would not be visible on the scale of figure 12.

In the derivation of equation (4.8), Suzumura [35] explicitly uses the relations between the velocities v_ν and the coupling constants g_i satisfied by the Luttinger model. Suzumura discards $g_{4\parallel}$ on account of the Pauli principle. This argument, in fact, only holds for a local potential where $g_{4\parallel}(p)$ is independent of p, and neglecting $g_{4\parallel}$ is not permitted in general (the Luttinger model is not even well defined for a $\delta(x)$ potential). One can re-evaluate (4.8) in the presence of $g_{4\parallel}$ and find

$$\pi\Lambda\int_0^\infty \mathrm{d}\omega\left(N(\omega)-\frac{1}{\pi v_F}\right)=-\frac{g_{4\parallel}(p=0)}{2\pi v_F}. \tag{4.9}$$

Only $g_{4\parallel}(p=0)$ enters since the Green function (2.13) depends, to the (universal) logarithmic accuracy of equation (2.13), only on the $g_i(p=0)$. We have given in section 2 general arguments why $g_{4\parallel}(p=0)$ should vanish, implying that Suzumura's sum rule is generally valid for the Luttinger model. If one should impose finite $g_{4\parallel}(p=0)$, equation (4.9) seems to suggest a renormalization of the chemical potential. Since (4.8) depends on the particular relations between velocities and coupling constants of the Luttinger model, it need not be satisfied by any more general model having a Luttinger-liquid fixed point in that regime, and consequently the maximum of figure 12 need not appear there.

The physical significance of the sum rule (4.8) is more transparent upon inserting (4.2) and (2.10) into (4.8). It then translates into

$$G^{\mathrm{R}}(x=0,t=0^+)-G_0^{\mathrm{R}}(x=0,t=0^+)=0 \tag{4.10}$$

i.e. the very-short-time behaviour of the exact interacting retarded Green function G^{R} must not be changed by the interactions with respect to the Green function of free electrons G_0^{R}. This ensures that the high-energy physics of the model is treated correctly in G. More fundamentally even, $G^{\mathrm{R}}(x=0,t=0^+)$ is related via (2.11) to the fermionic anticommutator, and (4.8) then guarantees that no important feature of the canonical transformation used to diagonalize (2.1) and (2.6) has been lost in the further course of calculation. Very loosely speaking one could say that (4.8) ensures $G^{\mathrm{R}}(0,0^+)$ to be the 'canonically transformed $G_0^{\mathrm{R}}(0,0^+)$'.

We finally want to discuss the density of states of a modified Luttinger liquid whose charge degrees of freedom are massless and described by the charge part of the Hamiltonian (2.1), resp. (2.6), and thus by parameters $K_\rho(\gamma_\rho)$ and v_ρ but whose spin fluctuations are massive with a gap Δ_σ—for reasons that will become obvious below when experiments are discussed. Formally, the system has $\alpha=\infty$ then. Theoretically, such a situation can arise in a variety of models, e.g. the $U<0$ Hubbard model [45], the attractive extended Hubbard model [13], the Luther–Emery solution of the backscattering problem [46] as well as for electrons interacting with acoustic [47] and intramolecular phonons [48].

The Green function $G(x=0,t)$ for this problem cannot be calculated exactly. The charge part of G is given by the charge parts of equations (2.13) or (2.15). For the spin part, a realistic guess or approximation has to be made. For this purpose, we borrow from the textbook example of a gapped many-body system, namely superconductivity, the diagonal parts of the Green function matrix ([37], equation (51.30)) and transform it into

$$G(k,t)=-\frac{\mathrm{i}}{2}\left[\theta(t)\exp[-\mathrm{i}(\xi_k^2+\Delta_\sigma^2)t^{1/2}]\left(1+\frac{\xi_k}{(\xi_k^2+\Delta_\sigma^2)^{1/2}}\right)\right.$$
$$\left.-\theta(-t)\exp[-\mathrm{i}(\xi_k^2+\Delta_\sigma^2)t^{1/2}]\left(1-\frac{\xi_k}{(\xi_k^2+\Delta_\sigma^2)^{1/2}}\right)\right] \tag{4.11}$$

with $\xi_k=v_F(rk-k_F)$. The $\langle c_k(t)c_k^+(0)\rangle$ and $\langle c_k^+(0)c_k(t)\rangle$ pieces are clearly separated here. One must now multiply these pieces separately by the corresponding charge contributions

in (2.13) or (2.15) to obtain the correct retarded Green function. We then interchange the integrations over t and ξ_k and perform the one over t first with the result (up to constants)

$$N(\omega) \sim \int_{-\infty}^{\infty} d\xi_k\, \theta[\omega - (\xi_k^2 + \Delta_\sigma^2)^{1/2}] \times \exp\left(-\frac{\Lambda}{v_\rho}[\omega - (\xi_k^2 + \Delta_\sigma^2)^{1/2}]\right)[\omega - (\xi_k^2 + \Delta_\sigma^2)^{1/2}]^{2\gamma_\rho - 1/2} \times {}_1F_1\left(\frac{1}{2}, 2\gamma_\rho + \frac{1}{2}; \frac{\Lambda}{v_\rho}[\omega - (\xi^2 + \Delta_\sigma^2)^{1/2}]\right) + (\omega \to -\omega) \tag{4.12}$$

where ${}_1F_1(a, b; z)$ is the confluent hypergeometric function [38]. It is clear that $N(\omega) = 0$ for $|\omega| < \Delta_\sigma$. This contradicts an earlier calculation [44], which finds a finite density of states in the gap and even at $\omega = 0$. We believe that the difference is due to our multiplying separately charge and spin in the particle and hole parts of the Green functions and building the total Green function out of these products, while Schulz apparently multiplies the charge and spin functions.

Also interesting is the onset of $N(\omega)$ close to Δ_σ. We find for the dominant term

$$N(\omega) \sim \theta(|\omega| - \Delta_\sigma)(|\omega| - \Delta_\sigma)^{2\gamma_\rho}. \tag{4.13}$$

The typical $(|\omega| - \Delta)^{-1/2}$ singularity of gapped 1D quantum systems, here present in the spin sector, is completely wiped out by the remaining massless charge fluctuation through the convolution of both parts in the density of states. Thus, in principle, the charge correlation exponent can be determined from the onset of $N(\omega)$ near Δ_σ. Notice that $\gamma_\rho \geqslant 0$ so that one expects a step function for free charges and a weaker singularity as correlations in the charge channel increase. The physical interpretation of the zero density of states for $|\omega| < \Delta_\sigma$ is most transparent in the $U < 0$ Hubbard model: the particles form bound singlet pairs, and such pairs must be broken in a photoemission experiment requiring a minimum energy Δ_σ.

Finally the half-filled 1D Hubbard model is symmetric under a simultaneous exchange $U \leftrightarrow -U$, $\rho \leftrightarrow \sigma$. Furthermore spin-rotation invariance requires for $U > 0$, $\gamma_\sigma = 0$, so that one would expect an edge discontinuity in $N(\omega)$ at the charge gap.

5. Photoemission experiments on one-dimensional materials

The results presented above should be directly relevant for photoemission experiments on quasi-1D systems thought to be describable as Luttinger liquids. There has recently been a series of experiments on organic and inorganic quasi-1D materials whose salient features will be summarized in the following. We do not pretend to have elaborated a theory for photoemission in these materials, but simply discuss to what extent they are consistent with a Luttinger-liquid hypothesis.

The organic conductors and superconductors of the $(TMTSF)_2X$ series (Bechgaard salts) are prime candidates in this field. They are in general metallic down to quite low temperature, where they undergo a spin-density wave (SDW) or superconductivity transition. There is evidence for important repulsive interactions and sizable anisotropy in the electronic properties. Moreover NMR experiments have already been analysed in a Luttinger-liquid picture [23, 24].

A high-resolution photoemission experiment was recently performed on the system with the counterion $X=PF_6$ [28] in its normal state at 50 K. The experiment had an

excellent energy resolution but the angular resolution was less good, so that, in principle, our predictions of section 3 have to be integrated over a finite k-domain in order to be comparable with the experiment. In this situation, one would expect, loosely speaking, to see the shape of the spectral weight near its onset more similar to that of $N(\omega)$, figure 12, at least on a frequency scale $v_F\Delta k$ where Δk is the resolution, but the signal should disperse in a manner indicative of the angle-resolved functions. The experiments could not detect any signature of a Fermi edge (indicative of divergent response in the angle-resolved functions $\rho(q,\omega)$). Only a broad prominent feature near -1 eV, i.e. at the very bottom of or even outside the conduction band of $(TMTSF)_2PF_6$, was detected. There was no dispersion of the measured signal upon varying the angles.

Similar behaviour is observed above the Peierls transition temperature in some inorganic quasi-1D charge-density wave (CDW) materials such as $(TaSe_4)_2I$ [25, 27] or $K_{0.3}MoO_3$ [25, 26]; only in $(TaSe_4)_2I$ is a dispersive signal seen [27], which, however, fades away as it approaches the Fermi energy. On the other hand, a clear signature of a Fermi edge is visible in the more 2D system 1T-TaS_2 [49].

Alternative models have been discussed in the original papers. Here we shall concentrate on the possible (in-?)consistency with a Luttinger-liquid picture. We concentrate on the Bechgaard salts.

The experiments are manifestly inconsistent with the results of sections 3 and 4 if one considers α values for the Luttinger liquid appropriate for e.g. the Hubbard model, $\alpha < 0.125$. In the density of states one expects a pronounced pseudo-Fermi edge—the $|\omega|^\alpha$ singularity will not be distinguishable from a step function in particular when thermal broadening is included. Moroever, angle-resolved experiments should see two dispersing peaks corresponding to energies $v_\nu q$ where the momentum transfer q onto the chain is varied with the angle. None of these properties are observed.

The experiments are more consistent, however, with our results if one assumes large values of α in excess of unity indicative of strong and long-range interactions. In this case, the density of states starts off the Fermi surface with a flat tangent and gradually rises towards lower energies. It exhibits a maximum at finite energies whose precise location, however, cannot be determined within the model (it depends on the cut-off and therefore requires a more complete theory—or unambiguous experimental identification). The possibility of shift of spectral weight over significant energies is also borne out by our calculations, although we cannot determine whether it appears inside or outside the conduction band. However, an identification of the experimental maximum with the one in figure 12 is certainly not permitted for a variety of reasons: (i) The Luttinger-liquid picture is likely to become irrelevant on energy scales of the order of the (real) bandwidth and more complete models must be used. (ii) Quantum-chemical calculations indicated the existence of molecular orbitals below the conduction band in this energy range [50]. (iii) Evidence for the presence of such orbitals in this energy range has also been provided in earlier photoemission experiments on TTF-TCNQ [51]. Still, the experiments do not show signatures of the spectral weight associated with the conduction band at energies smaller than 1 eV and apparently constrain the ground state of any more realistic theory to be of the large-α Luttinger-liquid type.

Also the absence of prominent dispersive features in angle-resolved experiments is consistent with a large-α Luttinger-liquid picture. It is obvious from figure 10(b) that no strong feature is observed near $v_\sigma q$, rather a smooth rise in spectral weight, which renders the detection of the dispersing onset impossible. Moreover, at $v_\rho q$ there is just an upward cusp whose experimental detectability is questionable: with a finite k-space resolution Δk,

$\rho(q,\omega)$ is integrated over a width Δk, sharp features are thus averaged over Δk and weak singularities may be wiped out completely if Δk is not really small.

In the large-α regime, spectral weight is pushed away from $v_\nu q$ and appears shifted to higher energies, typically a fraction of v_F/Λ. The evaluation of $\rho(q,\omega)$ for the spinful problem is affected by the approximation involved, over this energy range. Since charge–spin separation is not 'important' at these high values of α, the problem can as well be discussed for the spinless model, where exact results have been given. Figure 7(b) shows that, for large α, so long as $q \lesssim 1$ (in units of Λ^{-1}), the maximum in spectral response is at frequencies of order $\omega \sim v_F/\Lambda$ independent of q. Dispersion only sets in for $q \gg 1$.

The Luttinger liquid is a phenomenological picture. As such, its main shortcoming is its inability to provide a microscopic picture for the origin of the interaction constants g_i but its principal virtue lies in the possibility to calculate all correlation functions and thus to tie together various experiments. Important insight into the electronic properties has been gained by NMR experiments [23, 24]. The temperature dependence of the spin–lattice relaxation rate T_1^{-1} is governed by an exponent $\alpha_{SDW} = 1 - K_\rho$ (named γ in Bourbonnais' work [23]) and can thus be related to the exponent α measured in photoemission. Recent experiments [24] give $\alpha_{SDW} \sim 0.85$, thus $K_\rho \sim 0.15$, and imply $\alpha \simeq 1.25$ consistent with the photoemission experiment.

Another prediction is that the CDW response at $4k_F$, characterized by an exponent $\alpha_{4k_F} = 2-4K_\rho$, is stronger than CDW and SDW at $2k_F$ with exponents $\alpha_{CDW} = \alpha_{SDW} = 1-K_\rho$ [9, 13, 21]: for $K_\rho = 0.15$, we find $\alpha_{4k_F} = 1.4 > \alpha_{SDW} = \alpha_{CDW} = 0.85$. The connection of this prediction with the experimental situation is, however, not clear to date. Diffuse x-ray scattering at $4k_F$ has not been observed in the $(TMTSF)_2X$ compounds—but has neither been observed in the related series $(TMTTF)_2X$ where $4k_F$ charge localization has been established quite convincingly. One might also be tempted to associate the observed room-temperature dimerization with the strong $4k_F$ response. However, the opposite evolution with temperature in the TMTSF and TMTTF series shows that the physics presumably is more complex [52].

With these caveats in mind, consistency of photoemission with a Luttinger-liquid picture requires to place the organic conductors of the TMTSF series in a regime of large $\alpha > 1$. Such values are far beyond the limits satisfied by the 1D Hubbard model [9, 10, 14, 31] and also the quarter-filled extended Hubbard model [53], and would indicate the presence of important long-range electronic interactions. Phonons also can contribute to an enhancement of α [47]. One would thus place the TMTSF compounds at the edge of a charge localization transition but still on the metallic side, while the interactions in the TMTTF series are stronger and would lead to localization. Evidence for important charge localization effects has been produced with infrared spectroscopy on some TMTSF compounds [54].

As a final comment, we address the apparent universality of the (absence of) spectral response in quasi-1D materials. While the electronic properties of the quasi-1D CDW materials are radically different from those of the organic superconductors, their photoemission properties are quite similar. In particular, electron–phonon coupling seems to be the dominant interaction in the CDW materials. Notice in this context that many electronic properties are determined by many-particle correlation functions, which depend on both sign and magnitude of the interactions (for some examples see below). The single-particle properties only depend on the interaction strength and are necessarily more symmetric. More importantly, we discussed at the end of the preceding section how a vanishing density of states over a finite energy range together with only weak singularities at onset naturally emerges in a 'paired Luttinger liquid' where mobile charges are described by a Luttinger Hamiltonian but the spins are gapped. There is ample experimental evidence for such a

(pseudo)gap in a variety of CDW materials and its persistence deep into the normal state [55], although the origin is usually sought in the thermal precursor fluctuations of the Peierls transition [56]. The charge–spin separated version suggested above is consistent with experiments on some compounds (e.g. $K_{0.3}Mo_{0.3}$) but not on others $(TaSe_4)_2I$ or $(FA)_2PF_6$ (FA stands for the organic molecule fluoranthene). There also seem to be more microscopic theories pointing towards such a picture [57].

6. Further developments and summary

In the preceding sections the influence of charge–spin separation and of power-law correlations on the single-particle spectral properties has been investigated, and the quite different consequences of both properties have emerged. When charge–spin separation is dominant, the spectral response is characterized by a double-peak structure and the bulk of the spectral weight is concentrated between the peaks. The anomalous correlations, on the other hand, produce a transfer of spectral weight to higher energies and generally weaken the observed divergences. In extreme cases, possibly even of experimental relevance, correlations may wipe out the spectral signatures of charge–spin separation.

The single-particle response is fully described by the two velocities v_ν and the exponent α. It does not depend strongly on the sign of the Luttinger interactions g_i since α is symmetric in g_2, and the v_ν are just interchanged under $g_i \to -g_i$. Many-particle correlation functions do depend on the sign of the interactions and it is therefore interesting to search for the effects of charge–spin separation there. Three density-wave correlation functions, which, in principle, can be studied by neutron scattering, are of particular interest: $2k_F$ CDW and SDW and $4k_F$ CDW. Their retarded correlation functions are defined as

$$R_j^R(x,t) = -i\theta(t)[O_j(xt), O_j^+(00)] \tag{6.1}$$

where the operators O_j are given in terms of the phase fields $\phi_\nu(x)$ and $\theta_\nu(x)$ by [13]

$$O_{CDW}(x) = \frac{\exp(-2ik_Fx)}{\pi\alpha}\exp[\sqrt{2}i\phi_\rho(x)]\cos[\sqrt{2}\phi_\sigma(x)] \tag{6.2a}$$

$$O_{SDW,z}(x) = i\frac{\exp(-2ik_Fx)}{\pi\alpha}\exp[\sqrt{2}i\phi_\rho(x)]\sin[\sqrt{2}\phi_\sigma(x)] \tag{6.2b}$$

with two similar expressions for the x and y components [13], and

$$O_{4k_F}(x) = \frac{\exp(-4ik_Fx)}{(\pi\alpha)^2}\exp[\sqrt{8}i\phi_\rho(x)]. \tag{6.2c}$$

CDW and SDW operators are products of a charge and a spin part and will therefore be sensitive to charge–spin separation in their dynamical properties while $4k_F$ CDW will not, involving solely charge degrees of freedom. The structure factor close to $2k_F$ is then given by

$$S(2k_F+q,\omega) = \frac{-1}{\pi}\operatorname{Im} R_{CDW}^R(2k_F+q,\omega) \tag{6.3}$$

$$= \frac{\Lambda^{K_\rho+K_\sigma-2}}{2\pi^3}\int_\infty^\infty dx\int_\infty^\infty dt\, e^{i(\omega t-qx)}\Bigg(\prod_{\nu=\rho,\sigma}[(\alpha+iv_\nu t)^2+x^2]^{-1/2}$$

$$\times[(\Lambda+iv_\nu t)^2+x^2]^{(1-K_\nu)/2}+(x\to -x, t\to -t)\Bigg). \tag{6.4}$$

Equivalent expressions are obtained for the magnetic structure factor $\chi(2k_F+q,\omega)$ (here $K_\sigma \to K_\sigma^{-1}$ for the x and y components of the spins) and for the $4k_F$ structure factor (simply replace all (K_σ, v_σ) by another (K_ρ, v_ρ)). The exponents of the previous section are $\alpha_{SDW,z} = \alpha_{CDW} = 2-K_\rho-K_\sigma \to 1-K_\rho$ for spin-rotation invariance, and $\alpha_{4k_F} = 2-4K_\rho$. We do not attempt an exact evaluation of these functions but will only discuss their properties qualitatively. The term in large parentheses in (6.4) is symmetric under separate interchange of $x \to -x$ and $t \to -t$, implying independent symmetries of the structure factor under $\omega \to -\omega$ and $q \to -q$. Analyticity considerations similar to those in section 3 show that the structure factor vanishes for $-v_\sigma q < \omega < v_\sigma q$ ($v_\sigma < v_\rho$ assumed). Moreover, $S(2k_F+q,\omega)$ will exhibit power-law singularities at $\pm v_\nu q$ whose exponents can be determined by power counting. We find

$$S(2k_F+q, \omega \simeq \pm v_\sigma q) \sim \theta(|\omega|-v_\sigma q)(|\omega|-v_\sigma q)^{K_\rho+K_\sigma/2-1} \tag{6.5}$$

and

$$S(2k_F+q, \omega \simeq v_\rho q) \sim ||\omega|-v_\rho q|^{K_\rho/2+K_\sigma-1}. \tag{6.6}$$

The symmetry of the exponents in (6.5) and (6.6) is a consequence of the symmetry of charge and spin degrees of freedom manifest in (6.4).

The magnetic structure factor $\chi(2k_F+q,\omega)$ is governed by the same exponents as $S(2k_F+q,\omega)$, and

$$S(4k_F+q, \omega \simeq v_\rho q) \sim \theta(|\omega|-v_\rho q)(|\omega|-v_\rho q)^{2K_\rho-1}. \tag{6.7}$$

For $K_\sigma = 1$ and $K_\rho \leqslant 1$ there are only cusp singularities at $\pm v_\nu q$ in the structure factors. As K_ρ decreases (the interactions become more repulsive) the cusps will become more pronounced and, as K_ρ falls below 1/2 (notice in passing $K_\rho \geqslant 1/2$ for the repulsive Hubbard model [9, 10, 14]), divergences will simultaneously appear at $\omega = \pm v_\sigma q$ in $S(2k_F+q,\omega)$ and $\chi(2k_F+q,\omega)$ and at $\omega = \pm v_\rho q$ in $S(4k_F+q,\omega)$, while the cusp will only sharpen at $\pm v_\rho q$ in the $2k_F$ functions.

Apparently, the many-particle correlation functions produce complementary information on the effective interactions close to the Fermi surface, to that provided by the single-particle properties.

Not only do they depend on the sign of the interactions ($K_\nu > 1$ for attraction and $K_\nu < 1$ for repulsion) but the range of coupling constants where strong divergences are produced are opposite: while the single-particle properties diverge most strongly for weak coupling ($\alpha \ll 1$, i.e. $K_\rho \sim 1$), the many-particle properties such as the charge or magnetic structure factors show their strongest divergences only at strong coupling, and by comparing, for $K_\rho < \frac{1}{2}$, $\chi(2k_F+q,\omega)$ with $S(4k_F+q,\omega)$ a fairly accurate picture of the importance of charge–spin separation could be obtained. Were it not for the tiny sample size, neutron scattering experiments on the Bechgaard salts would be most instructive since the photoemission and NMR experiments discussed above seem to locate $K_\rho \sim 0.15$, i.e. strong divergences are expected in the different structure factors.

Apart from experimental verification, it may also be interesting to check the predictions of this paper by computer simulation. It is then important to choose carefully the model to be studied depending upon the method used. For example, in the world-line Monte Carlo method [58] the calculation of single-particle properties is difficult because it amounts to interrupting fermion world lines. Two- and four-particle correlation functions require, however, $K_\rho < \frac{1}{2}$ for strong divergences; thus the Hubbard model will probably not produce structured results and should be avoided in favour of models with longer-range interactions.

The situation is opposite for algorithms evaluating directly the Green function [59] where single-particle properties are readily obtained. Here, the Hubbard model will probably produce the clearest results, and the predictions of section 3 should then be open to numerical verification.

To summarize, we have studied in this paper the spectral properties of the single- and many-particle correlation functions of Luttinger liquids. We have attempted specifically to separate the influences of charge–spin separation and power-law correlations. Charge–spin separation generally produces a double-singularity structure in the spectral functions at $\omega = v_\nu q$. Non-universal divergences there are caused by the anomalous fermion dimensions as well as a shift of spectral weight to higher energies. Single-particle and many-particle functions are complementary in that charge–spin separation is most apparent in the single-particle properties at smaller interaction strength and/or range while the opposite is true for the two-particle correlation function. In any case, charge–spin separation can only be probed by angle-resolved experiments where the full dynamical correlations $\rho(q, \omega)$ are probed.

Acknowledgments

Many people have contributed to the maturation of the ideas and results in this paper. I wish to thank in particular M Fabrizio, B Fourcade, T Hsu, D Malterre, C Misbah, P Nozières, J P Pouget, P Quémerais, K Schönhammer, N Schopohl, H J Schulz and J Wheatley, and F Parisot for patiently and carefully performing the laborious typing of the manuscript.

References

[1] Sólyom J 1979 *Adv. Phys.* **28** 201
[2] Su W P, Schrieffer J R and Heeger A J 1980 *Phys. Rev.* B **22** 2099
[3] Tomonaga S 1950 *Prog. Theor. Phys.* **5** 544
[4] Luttinger J M 1963 *J. Math. Phys.* **4** 1154
[5] Mattis D C and Lieb E H 1963 *J. Math. Phys.* **6** 304
[6] Dzyaloshinkii I E and Larkin A I 1974 *Sov. Phys.–JETP* **38** 202
[7] Haldane F D M 1980 *Phys. Rev. Lett.* **45** 1358
[8] Haldane F D M 1981 *J. Phys. C: Solid State Phys.* **14** 2585
[9] Schulz H J 1990 *Phys. Rev. Lett.* **64** 2831
[10] Frahm H and Korepin V E 1990 *Phys. Rev.* B **42** 10553
[11] Ogata M, Luchini M, Sorella S and Assaad F F 1991 *Phys. Rev. Lett.* **66** 2388
[12] Hellberg C S and Mele E J 1991 *Phys. Rev. Lett.* **67** 2080
[13] Voit J 1992 *Phys. Rev.* B **45** 4027
[14] Anderson P W and Ren Y R 1990 *Proc. Los Alamos Symp. on High-T_c Superconductivity* (Reading, MA: Addison-Wesley) p 3
[15] Anderson P W 1990 *Phys. Rev. Lett.* **64** 1839 and **65** 2306
[16] Olson C G, Liu R, Lynch D W, List R S, Arko A J, Veal B W, Chang Y C, Jiang P Z and Paulikas A P 1990 *Phys. Rev.* B **42** 381
[17] Schulz H J 1991 *Int. J. Mod. Phys.* **5** 57
[18] Bourbonnais C and Caron L G 1991 *Int. J. Mod. Phys.* **5** 1033
[19] Valentí R and Gros C 1992 *Phys. Rev. Lett.* **68** 2402
[20] Pouget J P, Khama S K, Denoyer F, Comès R, Garito A F and Heeger A J 1976 *Phys. Rev. Lett.* **37** 437
[21] Emery V J 1976 *Phys. Rev. Lett.* **37** 107
[22] Basista H, Bonn D A, Timusk T, Voit J, Jérôme D and Bechgaard K 1990 *Phys. Rev.* B **42** 4088
[23] Bourbonnais C, Creuzet F, Jérôme D, Bechgaard K and Moradpour A 1984 *J. Physique Lett.* **45** L755
[24] Wzietek P, Creuzet F, Bourbonnais C, Jérôme D, Bechgaard K and Batail P 1993 *J. Physique* I **3** 171
[25] Dardel B, Malterre D, Grioni M, Weibel P, Baer Y and Lévy F 1991 *Phys. Rev. Lett.* **67** 3144

[26] Dardel B, Malterre D, Grioni M, Weibel P, Baer Y, Schlenker C and Petroff Y 1992 *Europhys. Lett.* **19** 525
[27] Hwu Y, Almèras P, Marsi M, Berger H, Lévy F, Grioni M, Malterre D and Margaritondo G 1992 *Phys. Rev.* B **46** 13 624
[28] Dardel B, Malterre D, Grioni M, Weibel P, Baer Y, Voit J and Jérôme D 1993 *Phys. Rev. Lett.* submitted
[29] Voit J 1993 *Phys. Rev.* B **47** 6740
[30] Meden V and Schönhammer K 1992 *Phys. Rev.* B **46** 15 753
[31] Ogata M and Shiba H 1990 *Phys. Rev.* B **41** 2326
[32] Balatsky A and Stone M 1991 *Phys. Rev.* B **43** 8038
[33] Gebhard F and Ruckenstein A 1992 *Phys. Rev. Lett.* **68** 244
[34] Heidenreich R, Seiler R and Uhlenbrock D A 1980 *J. Stat. Phys.* **22** 27
[35] Suzumura Y 1980 *Prog. Theor. Phys.* **63** 5
[36] Luther A and Peschel I 1974 *Phys. Rev.* B **9** 2911
[37] Fetter A L and Walecka J D 1971 *Quantum Theory of Many-Particle Systems* (New York: McGraw-Hill) ch 7
[38] Whittaker and Watson 1927 *A Course of Modern Analysis* 4th edn (Cambridge: Cambridge University Press)
[39] Gradshteyn I S and Ryzhik I M 1980 *Table of Integrals, Series and Products* (New York: Academic)
[40] Magnus W, Oberhettinger F and Soni R P 1966 *Formulas and Theorems for the Special Functions of Mathematical Physics* (Berlin: Springer) p 274
[41] Schönhammer K and Meden V 1992 unpublished work
[42] Luttinger J M 1960 *Phys. Rev.* **119** 1153
[43] Gutfreund H and Schick M 1968 *Phys. Rev.* **168** 418
Brech M, Büttner H and Voit J 1990 *Europhys. Lett.* **12** 289
[44] Schulz H J 1983 *Thèse d'Etat* Université Paris-Sud
[45] Bahder T B and Woynarovich F 1986 *Phys. Rev.* B **33** 2114
[46] Luther A and Emery V J 1974 *Phys. Rev. Lett.* **33** 589
[47] Voit J and Schulz H J 1988 *Phys. Rev.* B **37** 10 068
[48] Voit J 1990 *Phys. Rev. Lett.* **64** 323
[49] Dardel B, Grioni M, Malterre D, Weibel P, Baer Y and Lévy F 1992 *Phys. Rev.* B **46** 7907
[50] Minot C and Louie S G 1982 *Phys. Rev.* B **26** 4793
[51] Grobman W D, Pollak R A, Eastman D E, Maas E T and Scott B A 1974 *Phys. Rev. Lett.* **32** 534
[52] Gallois B, Gaultier J, Hauw C, Lamcharfi T-D and Filhol A 1986 *Acta Crystallogr.* B **42** 564
[53] Mila F and Zotos X 1993 *Preprint* Neuchâtel
[54] Bozio R, Meneghetti M, Pedron D and Pecile C 1988 *Synth. Met.* **27** B 129
[55] Johnston D C 1984 *Phys. Rev. Lett.* **52** 2049
[56] Lee P A, Rice T M and Anderson P W 1973 *Phys. Rev. Lett.* **31** 462
[57] Quémerais P 1993 Private communication
Aubry S and Quémerais P 1989 *Low-Dimensional Electronic Properties of Molybdenum Bronzes and Oxides* ed C Schlenker (Dordrecht: Kluwer) p 295
[58] Hirsch J E, Scalapino D J, Sugar R L and Blankenbecler R 1981 *Phys. Rev. Lett.* **47** 1628
[59] Hirsch J E 1983 *Phys. Rev. Lett.* **51** 1900